Acta Neuropathologica (2025) 149:9
https://doi.org/10.1007/s00401-025-02844-z

ORIGINAL PAPER

Comparison of the amyloid plaque proteome in Down syndrome, early-onset Alzheimer's disease, and late-onset Alzheimer's disease

Mitchell Martá-Ariza[1,2,3] · Dominique F. Leitner[1,2,4] · Evgeny Kanshin[5,6] · Jianina Suazo[1,2] · Ana Giusti Pedrosa[7] · Manon Thierry[1,2] · Edward B. Lee[8] · Orrin Devinsky[1,4] · Eleanor Drummond[2,9] · Juan Fortea[10,11,12] · Alberto Lleó[10,11] · Beatrix Ueberheide[1,5,6] · Thomas Wisniewski[1,2,13,14]

Received: 8 November 2024 / Revised: 2 January 2025 / Accepted: 4 January 2025

Abstract

Down syndrome (DS) is strongly associated with Alzheimer's disease (AD) due to *APP* overexpression, exhibiting Amyloid-β (Aβ) and Tau pathology similar to early-onset (EOAD) and late-onset AD (LOAD). We evaluated the Aβ plaque proteome of DS, EOAD, and LOAD using unbiased localized proteomics on post-mortem paraffin-embedded tissues from four cohorts ($n = 20$/group): DS (59.8 ± 4.99 y/o), EOAD (63 ± 4.07 y/o), LOAD (82.1 ± 6.37 y/o), and controls (66.4 ± 13.04). We identified differentially abundant proteins when comparing Aβ plaques and neighboring non-plaque tissue (FDR < 5%, fold-change > 1.5) in DS ($n = 132$), EOAD ($n = 192$), and LOAD ($n = 128$), with 43 plaque-associated proteins shared across all groups. Positive correlations were observed between plaque-associated proteins in DS and EOAD ($R^2 = .77$), DS and LOAD ($R^2 = .73$), and EOAD and LOAD ($R^2 = .67$). Top gene ontology biological processes (GOBP) included lysosomal transport ($p = 1.29 \times 10^{-5}$) for DS, immune system regulation ($p = 4.33 \times 10^{-5}$) for EOAD, and lysosome organization ($p = 0.029$) for LOAD. Protein networks revealed a plaque-associated protein signature involving APP metabolism, immune response, and lysosomal functions. In DS, EOAD, and LOAD non-plaque vs. control tissue, we identified 263, 269, and 301 differentially abundant proteins, with 65 altered proteins shared across all cohorts. Non-plaque proteins in DS showed modest correlations with EOAD ($R^2 = .59$) and LOAD ($R^2 = .33$) compared to the correlation between EOAD and LOAD ($R^2 = .79$). Top GOBP term for all groups was chromatin remodeling ($p < 0.001$), with additional terms for DS including extracellular matrix, and protein–DNA complexes and gene expression regulation for EOAD and LOAD. Our study reveals key functional characteristics of the amyloid plaque proteome in DS, compared to EOAD and LOAD, highlighting shared pathways in endo/lysosomal functions and immune responses. The non-plaque proteome revealed distinct alterations in ECM and chromatin structure, underscoring unique differences between DS and AD subtypes. Our findings enhance our understanding of AD pathogenesis and identify potential biomarkers and therapeutic targets.

Keywords Down syndrome · Alzheimer's disease · Proteomics · Amyloid-β · Neuropathology

Introduction

Down syndrome (DS) is the most prevalent chromosomal abnormality, characterized by the partial or complete triplication of chromosome 21 (Hsa21) [3, 24]. DS is strongly associated with Alzheimer's disease (AD) due to the triplication of the amyloid-β precursor protein (*APP*) gene in Hsa21 [30, 39, 41]. Hsa21 also contains other genes of interest for AD, such as S100β (associated with astrocytes), *DYRK1A* (encodes for a kinase that phosphorylates Tau), and *SOD1* and *BACE2* (related to oxidative stress) [40, 91, 93, 127, 129], which may play a role in AD in addition to *APP*. By age 40, virtually, all individuals with DS exhibit AD pathological hallmarks, including extracellular amyloid-β (Aβ) accumulation and neurofibrillary tangles formed by hyperphosphorylated Tau [31, 102, 130]. Brain atrophy and elevated cerebrospinal fluid and plasma levels of Aβ42 and neurofilament light, respectively, have been observed in people with DS [36]. These neuropathological features are qualitatively similar to other AD forms, such as early (EOAD) and late-onset AD (LOAD) [2, 36].

Earlier investigations and most recent findings suggest that AD neuropathology extends beyond Aβ and Tau proteins [31, 81], implicating hundreds of associated proteins

Extended author information available on the last page of the article

Published online: 18 January 2025

in biological dysfunctions, such as synaptic transmission, immune response, mitochondrial metabolism, and oxidative stress [16, 25, 55]. Proteomic comparisons between DS and EOAD Aβ plaques reveal common proteins enriched in both conditions, although differences in protein abundance have been observed [31]. Despite recent progress, the molecular mechanisms of AD remain elusive, particularly regarding common pathophysiological mechanisms across AD subtypes and the specifics of AD neuropathogenesis in DS. Individuals with DS develop AD neuropathology earlier than the general AD population, with Aβ and Tau accumulation patterns mirroring those in AD [53]. However, the extent to which the protein composition in DS pathological lesions aligns with other AD subtypes remains uncertain [23]. Identifying gene–phenotype associations in DS is also challenging due to multiple triplicated genes [2]. Given these complexities, DS is particularly relevant as an AD model, due to the universal prevalence of DS with AD pathology with increasing age, compared to the other autosomal dominant inherited forms of AD and the more homogeneous, age-dependent pathology compared to LOAD [2, 37, 50, 109].

In light of these findings, this study aimed to characterize the proteomic differences among AD subtypes. In particular, we examined the Aβ plaque proteome in DS, EOAD, and LOAD, expanding on prior DS and EOAD comparisons [31]. Our analysis revealed a substantial similarity of proteins enriched in Aβ plaques across all experimental groups, providing new evidence about the Aβ plaque-protein composition of individuals with DS in direct comparison with EOAD and LOAD. The proteomes also shared functional associations, thus revealing a consistent plaque-protein signature in DS, EOAD, and LOAD. Despite the enrichment of similar plaque proteins in all cohorts, we observed subtle differences in the proteome composition, characterized by variations in protein abundance in each group. Corresponding observations were made in the proteomic composition of DS, EOAD, and LOAD non-plaque tissue compared to controls. These insights may contribute to identifying novel therapeutic targets or biomarkers tailored to the specific features of different AD subtypes.

Methods

Human brain tissue

Post-mortem formalin-fixed and paraffin-embedded (FFPE) brain tissues from DS, EOAD, LOAD, and cognitive normal age-matched controls ($n = 20$ brain cases for each cohort) were obtained from the National Institutes of Health NeuroBioBank (Maryland and Mt. Sinai brain banks), UK Brain Bank Network (South West Dementia brain bank), IDIBAPS Biobank from Barcelona, University of Pennsylvania and NYU Grossman School of Medicine, including autopsy tissues from NYU Alzheimer's Disease Research Center (ADRC), Center for Biospecimen Research and Development (CBRD)/Department of Pathology and the North American SUDEP Registry (NASR) at NYU Comprehensive Epilepsy Center (CEC). FFPE tissue blocks containing hippocampus and surrounding entorhinal and temporal cortex were used for the present study as it contains a high amount of amyloid pathology. The cases were assessed by the brain repositories to confirm advanced AD, by ABC neuropathological score [12, 84, 117]. Further details about the cases are included in Table 1 and detailed case history is provided in Supp. Table. 1. Cases lacking information about α-synuclein and TDP-43 were stained by CBRD and assessed in the laboratory. Inclusion criteria for all cases included tissue formalin fixation below 3 years. We tolerated cases with TDP-43 (DS = 2, EOAD = 2, LOAD = 1) or α-synuclein (DS = 7, EOAD = 2, LOAD = 1) inclusions to increase the number of cases, as these co-pathologies are common in the elderly population. We performed one-way ANOVA analysis followed by post hoc Tukey's multiple

Table 1 Case history summary

Group	Cases	Mean age at death (years)*	Sex	Mean PMI (hours)*	Neuropathology	*APOE* genotype
Down syndrome	20	59.8 ± 4.99	7 F/13 M	17.95 ± 11.71	Equivalent to A3, B3, C3 score or Braak V-VI, Thal 5	ε3/ε3: 13, ε4/ε4: 2, ε3/ε4: 3, ε2/ε4: 1
EOAD	20	63 ± 4.07	5 F/15 M	27.47 ± 12.76	Equivalent to A3, B3, C3 score or Braak V-VI, Thal 4	ε3/ε3: 10, ε4/ε4: 3, ε3/ε4: 5, ε2/ε3: 2
LOAD	20	# 82.1 ± 6.37	10 F/10 M	33.22 ± 19.19	A3, B3, C3 or Braak VI	ε3/ε3: 6, ε4/ε4: 3, ε3/ε4: 7, ε2/ε3: 2, ε2/ε4: 2
Control	20	66.4 ± 13.04	9 F/11 M	59.50 ± 27.30	≤ A1, B1, C1	N/A

*Mean age at death and mean PMI ± Standard deviation. #Significant differences by one-way ANOVA

comparison test to evaluate age differences among the cohorts and multiple variable linear regression to determine the influence of clinical traits age and sex in the proteomics results.

APOE genotyping

APOE genotyping was conducted for the cases where this information was not provided by the brain banks, following a previously established protocol [31]. Briefly, DNA extraction from FFPE tissue scrolls was performed using the QIAamp DNA FFPE Advanced UNG Kit (Qiagen, cat. 56,704) as indicated by the manufacturer. Two end-point PCRs were carried out using custom primers (forward primer 5′ AGGCCTACAAATCGGAACTGG 3′; reverse primer 5′ CCTGTTCCACCAGGGGC 3′; Sigma). After the initial PCR, DNA purification from the agarose gel was accomplished using the QIAquick Gel Extraction Kit (Qiagen, cat. 28,704), following the manufacturer's protocol. Subsequently, the gel-purified DNA was used for the second end-point PCR, followed by Sanger sequencing and sequence analysis using SnapGene 5.3.1 software.

Immunohistochemistry for Aβ and pTau

FFPE 8 µm tissue sections that contain the hippocampus and adjacent temporal cortex were collected on glass slides. Sections underwent chromogenic immunohistochemistry for total Aβ (Aβ 17–24 clone 4G8, 1:1000, BioLegend, cat. 800,710) and Tau pathology (PHF-1, 1:200, in house developed mouse monoclonal antibody provided by Dr. Peter Davies, Albert Einstein University, NY, USA [45]). Sections were deparaffinized and rehydrated through a brief series of xylene and ethanol washes. Antigen retrieval methods performed include a 7-min treatment of 88% formic acid followed by heat-induced citrate buffer treatment (10 mM sodium citrate, 0.05% Tween-20; pH 6). Endogenous peroxidase was quenched with 0.3% H_2O_2 solution for 20 min. Sections were blocked with 10% normal goat serum, followed by an overnight incubation with the primary antibody diluted in 4% normal goat serum. Sections were incubated for 1 h at room temperature with the appropriate secondary antibody (biotinylated HRP mouse IgG, 1:1000, Vector, cat. BA-2000). Staining signal was amplified using VECTASTAIN Avidin–Biotin Complex (ABC) kit (Vector, cat. PK6100) for 30 min. The chromogen DAB was used to visualize the pathology. Sections were counterstained with hematoxylin and coverslipped using the appropriate mounting media. Aβ and Tau quantities were quantified from whole slide scans at 20X magnification using a Leica Aperio Versa 8 microscope. Five regions of interest (ROIs) in the temporal cortex and hippocampus (CA1, CA2, CA3) were used to calculate the percent positive pixel area. We used a custom macro based on the 'Positive Pixel Count' algorithm in ImageScope v.12.4.3.5008, with a modification to the 'Color saturation threshold' = 0 and the 'Upper limit of intensity for weak-positive pixels' (Iwp high) = 190. Statistical differences between experimental groups were evaluated using one-way ANOVA followed by Tukey's post hoc multiple comparisons test in GraphPad Prism v 9.5.1. Data are shown as mean ± standard error of the mean (SEM).

Laser-capture microdissection

Unbiased localized proteomics was performed using the method outlined in Fig. 1a. FFPE tissues were cut into 8 µm sections from autopsy hippocampal and adjacent entorhinal and temporal cortex tissues onto laser-capture microdissection (LCM) compatible PET membrane slides (Leica, cat. 11,505,151). Amyloid-β deposits were visualized by immunohistochemistry using the pan-Aβ 4G8 antibody (1:1000, BioLegend, cat. 800,710), using the chromogen 3,3-diaminobenzidine (DAB, Thermo Scientific, cat. 34,065) reaction. Classic cored, neuritic and dense Aβ plaques were targeted (not diffuse or cotton-wool plaques) in gray matter of the hippocampal formation, and the adjacent subiculum and entorhinal cortex, as well as from the gray matter of the temporal cortex, in regions distant from the hippocampus, for a more homogeneous analysis, using LCM to dissect a total area of 2 mm^2 and the same area for neighboring non-plaque tissue (Fig. 1b–c), at 10X magnification with a LMD6500 microscope equipped with a UV laser (Leica). We avoided diffuse amyloid aggregates in all the cases used to maintain sample consistency. Microdissected samples were centrifuged for 2 min at 14,000 g and stored at − 80 °C. We also microdissected adjacent tissue free of plaques from the same microscopic field of views that contained microdissected amyloid plaques, but at a sufficient distance from plaques to ensure that plaque-associated tissue was not collected (Fig. 1c). These samples are henceforth referred to as 'non-plaque'. In addition, analogous non-plaque tissue from control cases was selected from matching hippocampal and temporal cortex regions as those used in DS, EOAD, and LOAD, denoted as 'Control non-plaque'. The schematic diagrams for the figure were generated using BioRender.com.

Label-free quantitative mass spectrometry (MS) proteomics

The extraction and digestion of proteins from Laser-Capture Microdissection (LCM) excised plaque and non-plaque tissue samples were performed using the SPEED sample prep workflow [28]. Briefly, tissue sections were incubated in 10 µl of LC–MS grade formic acid (FA) for 5 min at 73 °C. The FA was then neutralized by a tenfold dilution with 2 M TRIS containing 10 mM Tris (2-carboxyethyl) phosphine

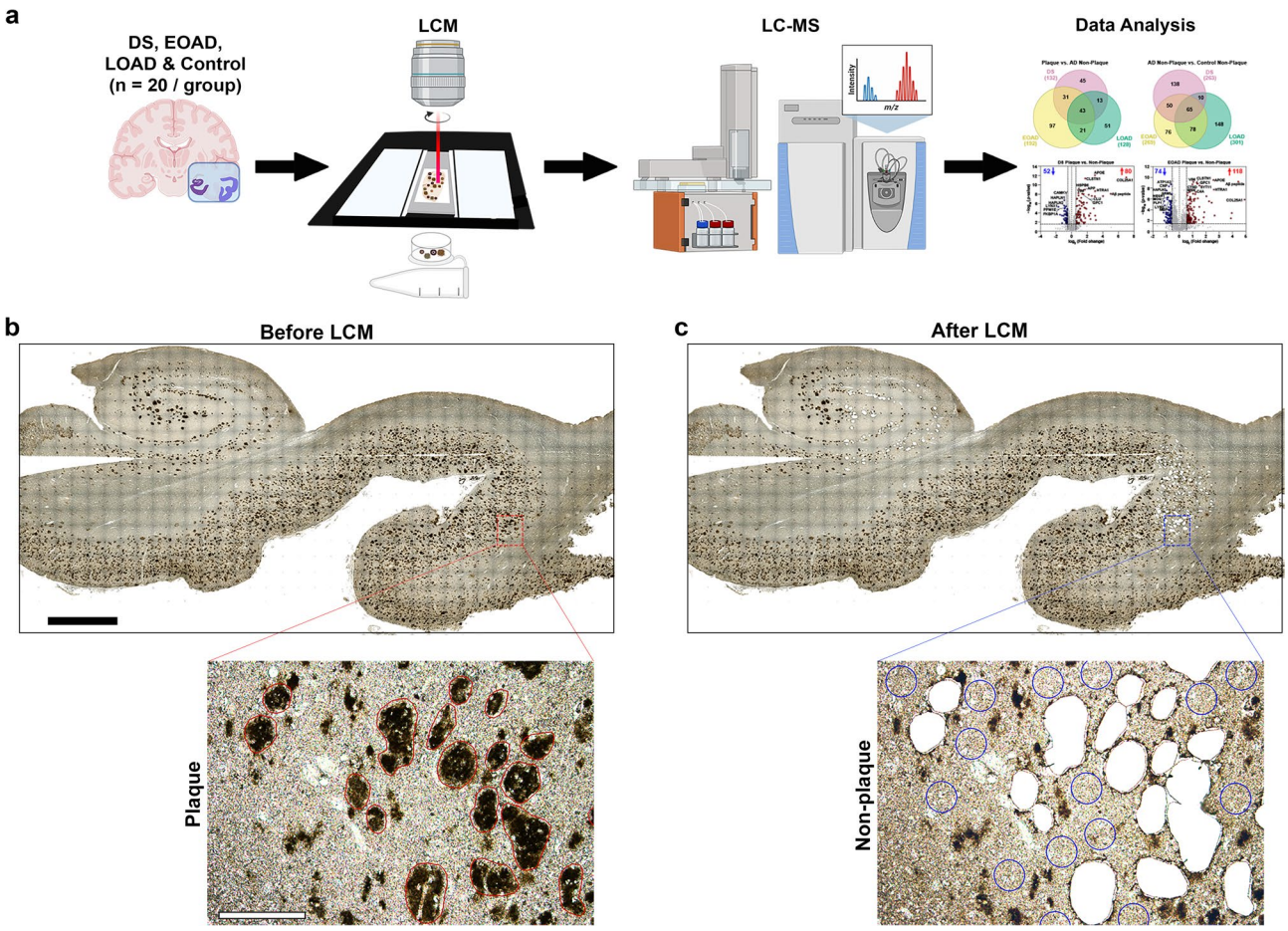

Fig. 1 Schematic of the localized proteomics protocol. **a** Laser-capture microdissection of 2 mm^2 total area of amyloid-β plaques from hippocampus and adjacent temporal cortex from FFPE autopsy brain tissue from control, DS, EOAD, and LOAD ($n = 20$ cases/experimental group). Amyloid plaque proteins were quantified by label-free mass spectrometry and posteriorly analyzed. **b–c** Microphotographs of a typical brain tissue section immunolabeled against Aβ illustrate the precise microdissection of amyloid plaques before (**b**) and after LCM (**c**). 2 mm (black bar, top) and 200 µm (white bar, bottom)

(TCEP) and 20 mM chloroacetic acid (CAA), followed by an incubation at 90 °C for 1 h. For enzymatic digestion, samples were diluted sixfold with water containing 0.2 µg of sequencing-grade trypsin. Digestion was carried out overnight at 37 °C and halted by acidification to 2% TFA.

Liquid chromatography–tandem mass spectrometry (LC–MS/MS) was performed online on an Evosep One LC using a Dr. Maisch ReproSil-Pur 120 C18 AQ analytical column (1.9-µm bead, 150 µm ID, 15 cm long). Peptides were gradient eluted from the column directly into an Orbitrap HF-X mass spectrometer using the 88-min extended Evosep method (SPD15) at a flow rate of 220 nl/min. The mass spectrometer was operated in data-independent acquisition (DIA) mode, acquiring MS/MS fragmentation across 22 m/z windows after every MS full-scan event.

High-resolution full MS spectra were acquired with a resolution of 120,000, an Automatic Gain Control (AGC) target of 3e6, a maximum ion injection time of 60 ms, and a scan range of 350–165 m/z. Following each full MS scan, 22 data-independent higher-energy collisional dissociation (HCD) MS/MS scans were acquired at a resolution of 30,000, an AGC target of 3e6, and a stepped normalized collision energy (NCE) of 22.5, 25, and 27.5.

Proteomics computational analysis

The analysis of the MS data was conducted utilizing the Spectronaut software (https://biognosys.com/shop/spectronaut), searching in direct-DIA mode (w/o experimental spectral library) against the *Homo Sapiens* UniProt database (http://www.uniprot.org/) combined with a list of common laboratory contaminants. The integrated search engine Pulsar was employed for the database search. The enzyme specificity was configured to trypsin, allowing for up to two missed cleavages during the search process. The search also included oxidation of methionine as a variable modification,

and carbamidomethylation of cysteines as a fixed modification. The false discovery rate (FDR) for identification of peptide, protein, and site was limited to 1%. Quantification was performed on the MS/MS level, utilizing the three most intense fragment ions per precursor. Independent quantification of Aβ was manually curated and incorporated into the search results, consistent with previous studies [31, 71, 106]. The intensity of Aβ was quantified by integrating the area under the curve for the peptide LVFFAEDVGSNK, which corresponds to amino acids 17–28 of Aβ. This peptide does not differentiate between cleaved or full-length sequences but shows strong enrichment and correlation with Aβ pathology [31, 49, 72, 106]. Data were log-transformed and normalized using median intensity across all samples. For subsequent data analysis, the Perseus [119], R environment (http://www.r-project.org/), or GraphPad Prism were used for statistical computing and graphical representation.

Proteomics statistical analyses

The protein expression matrix ($n = 2080$) was filtered to remove common laboratory contaminants, non-human proteins, and those proteins observed in less than half of all the four groups evaluated ($n = 1995$). For principal component analysis (PCA), missing values were imputed from the normal distribution with a width of 0.3 and a downshift of 1.8 (relative to measured protein intensity distribution) using Perseus v 1.6.14.0 [119]. We performed paired *t* tests to evaluate the amyloid plaques enrichment in relation to the non-plaque tissue adjacent to the amyloid plaques. In addition, we performed unpaired *t* tests to compare the protein enrichment of non-plaques from DS, EOAD, and LOAD compared to control tissue samples. Proteins were deemed significantly altered if they had a false discovery rate (FDR) below 5% (permutation-based FDR with 250 data randomizations). We further filtered the significant proteins based on the fold-change (FC) difference > 1.5 fold between the groups. The proteins of interest common to each pairwise comparison from 'plaques vs. non-plaque' and 'non-plaque vs. control non-plaque' tissue were evaluated by Venn diagrams generated from InteractiVenn [54]. Pearson's correlation analysis between DS, EOAD, and LOAD differentially abundant proteins identified in the pairwise comparisons were evaluated using GraphPad Prism v 9.5.1. For this analysis, we considered proteins that were significantly altered in at least one of the groups and had an FC > 1.5, on a given correlation.

Mapping protein-coding genes to human chromosomes

Genes coding for the proteins identified in the study were mapped to their respective chromosomes in R using the function 'mapIds' from the *Annotation DBI* package v 1.62.2 with the genome-wide annotation for human, org.Hs.eg.db v 3.17.0. Percentage of significantly altered proteins was calculated by dividing the number of significant proteins per each chromosome by the total number of proteins mapped to the respective chromosome. Location for each protein-coding gene in the chromosome 21 (*Homo sapiens* autosome 21, or Hsa21) was determined using the UCSC Human Genome Browser [68].

Gene Ontology functional annotation

Gene Ontology (GO) enrichment analysis was performed in R using the function *enrichGO* from the package *clusterProfiler* v 4.8.2, with the genome-wide annotation for human, org.Hs.eg.db v 3.17.0. GO terms were filtered to an FDR < 0.05 using the Benjamini–Hochberg method [9]. Isoform labels were excluded from Uniprot accession IDs for GO functional annotation. Duplicate proteins were removed, and the resulting list comprising 1980 proteins lacking isoforms was utilized as the background dataset. Functional annotation was focused on GO biological process (GO BP) and GO cellular component (GO CC). Heavily redundant GO terms were reduced using the *simplify* function from clusterProfiler, with a cutoff of 0.7. Top ten significantly enriched GO terms for highly abundant proteins in 'plaques vs. non-plaque' and 'non-plaque vs. control non-plaque' for each experimental group were selected using the adjusted *p* value ($-\text{Log}_{10}$ adj. *p* value) and compared using heatmaps generated in GraphPad Prism.

Protein–protein interaction networks

Protein–protein interaction (PPI) networks were made in Cytoscape v 3.10.0 using 'STRING: protein query' (STRING v 11.5 database [114]) with a (high) confidence score of 0.7. Networks reflect functional and physical protein associations for the differentially abundant proteins in DS, EOAD, and LOAD. Node size of the networks indicate the adjusted *p* value ($-\log_{10}$ [*p* value]) from the *t* tests and node color indicates fold-change ($\log_2$ [FC]). Disconnected nodes were not depicted in the final network. Dotted-line colored boxes highlight proteins clustered by function similarity.

Comparison with previous AD proteomics studies in human brain

Our data were compared to previous proteomic studies using the NeuroPro database (v1.12; https://neuropro.biomedical.hosting/) [4]. NeuroPro is a combined analysis of differentially enriched proteins found in human AD brain tissues identified in 38 published proteomics studies (at the time of use for this study, February 2024). NeuroPro database was

filtered to include only proteins found in advanced AD proteomics studies (AD and AD/C). Alternatively, we applied a second filter to advanced AD to include proteomics studies in 'plaques' only. Protein lists obtained after filtering the NeuroPro database were manually curated to address current 'obsolete deleted', 'merged' or 'demerged' UniProt accession IDs. We performed a manual curation of NeuroPro protein lists to provide an accurate comparison between the proteins identified in previous proteomics studies and our present study. The UniProt accession IDs and gene IDs from the proteins we identified in the current study were matched to the IDs from the NeuroPro to identify proteins that have not been previously associated with human AD and amyloid plaque proteomics.

Additionally, as the NeuroPro database does not include DS proteomics data, we compared our current DS plaque dataset with our previous DS plaque proteomics study [31]. We identified the common proteins using the whole data matrix of both studies, by comparing the Uniprot Accession ID and the Gene ID, to account for any identifier differences. Then, we identified the significantly altered proteins in each study; for our dataset, we defined significantly altered proteins by FDR ≤ 5% and a fold-change ≥ 1.5. In our previous study, significantly altered proteins were defined by $p < 0.05$ and a fold-change ≥ 1.5. For the comparison, we included the significantly abundant and significantly decreased plaque proteins. We evaluated common significant proteins from the datasets using Venn diagrams generated from InteractiVenn [54]. In addition, we performed Pearson's correlation analysis between datasets using GraphPad Prism v 9.5.1. For the correlation analysis, we considered proteins that were significantly altered in at least one of the datasets.

Validation of proteins of interest

The proteins chloride voltage-gated channel 6 (CLCN6) and the Tripeptidyl peptidase I (TPP1, also known as CLN2), which are enriched in Aβ plaques, were validated using immunohistochemistry (IHC). CLCN6 was selected due to its significantly high abundance in DS plaques, limited evidence of its presence in plaques and about its role in AD, and its previously described function in the central nervous system [13, 92]. TPP1 was selected as another lysosomal protein, which has been described in the previous human proteomics studies to be associated to Aβ plaques, but it has not been validated by IHC. For immunolabeling, 8 µm serial sections adjacent to those used for proteomic analysis were deparaffinized and rehydrated. Sections from six cases in each cohort were subjected to antigen retrieval in a microwave, using Tris–EDTA buffer (pH 9, Proteintech), diluted 1X for CLCN6, and sodium citrate buffer pH 6, followed by formic acid treatment for TPP1. Primary antibodies against CLCN6 (1:350, Thermo Scientific, cat. OSC00147W-100UL), TPP1 (1:100, Sigma-Aldrich, cat. HPA037709-100UL), and the pan-Aβ 4G8 antibody (1:1000) were incubated overnight, followed by Alexa Fluor 488 and 647 secondary antibodies (Thermo Scientific). Additionally, we performed a co-staining using MAP2 (1:200, BD Biosciences, cat. 556,320) and CLCN6 to assess cell specificity of CLCN6 expression. Whole-slide scans were acquired at 20X magnification using a Leica Aperio Versa 8 microscope.

For CLCN6 quantification, ten regions of interest (ROIs) from the same anatomical areas used for LCM were analyzed using a custom macro in ImageJ 1.54f. Briefly, a mask was generated to delineate the plaques area in the field of view, which was then applied to the CLCN6 channel to measure fluorescence intensity (total fluorescence = Integrated Density—[Area measured * Background mean gray value]) or the area occupied by CLCN6-positive objects using the "Measure" function. CLCN6-positive area was normalized to the total area of the plaques. Non-plaque CLCN6 area and fluorescence were measured by modifying the macro, where plaque ROIs were first subtracted from the CLCN6 channel before proceeding with the previously described quantification method. Significant differences were assessed using paired t tests (for comparisons between plaque and non-plaque tissue within the same case) or unpaired t tests (for comparisons between control non-plaque tissue and non-plaque tissue from DS, EOAD, or LOAD), with analyses performed using GraphPad Prism.

TPP1 was quantified using QuPath v 0.5.1. Briefly, 10 regions of interest (ROIs) were manually annotated from the gray matter of the hippocampal formation and temporal cortex. Aβ plaques were annotated using a pixel classifier, with a Gaussian prefilter, smoothing sigma of 2, and a threshold of 30. Objects below 350 μm^2 were filtered out from the final annotations. Non-plaque adjacent tissue was selected using the same classifier, but ignoring pixels above threshold and assigning the remaining pixels detected to the class "Non-plaques". TPP1-positive objects were annotated using a similar pixel classifier, with smoothing sigma of 1.5 and a threshold of 26. Objects below 20 μm^2 were filtered out for the final annotations. Density of protein TPP1 was calculated for positive immunolabeling inside plaques and for presence of TPP1 in the non-plaque region, using the formula TPP1 density = (sum of TPP1 areas/sum of plaques area) × 100. T tests' statistical analyses were performed in GraphPad Prism.

Weighted gene correlation network analysis

We used the *WGCNA* package (version 1.72.1) in the R environment to conduct a Weighted Gene Correlation Network Analysis adapted from the WGCNA framework [137] to investigate protein expression correlations. First, the curated protein expression matrix from the proteomics

analysis ($n = 1995$) underwent quality control to identify samples with excessive missing values. The networks were then constructed using the *blockwiseModules* function for each cohort (DS, EOAD, and LOAD), creating separate networks for Aβ plaques and non-plaque tissue within each cohort. The networks were constructed as "signed networks" with the topological overlap matrix (TOM) also set to "signed". *TOMdenom* parameter was specified as "mean" to facilitate the capture of tightly connected protein groups within the network. The soft-thresholding power was set to 9 for DS Plaques and 10 for non-plaques, 7 for EOAD plaques and 11 for non-plaques, and 18 for LOAD plaques and 14 for LOAD non-plaque dataset. Additional parameters included a minimum module size of 10, a mergeCutHeight of 0.07 to merge highly similar modules more stringently, and a deepSplit value of 4 to facilitate finer differentiation of modules. A minimum intramodular connectivity (kME) of 0.3 was required for proteins to remain in a given module, with a reassignment threshold of 0.05 allowing minor reallocation of proteins to more appropriate modules if necessary. The biweight midcorrelation method (bicor) was used as the primary correlation measure, with a fallback to Pearson correlation for outlier adjustment where necessary (maxPOutliers = 0.1). Numeric module labels were employed for consistency, and to reduce the complexity of module visualization, the pamRespectsDendro option was set to FALSE.

After running the *blockwiseModules* function, we used the *signedKME* function within the WGCNA package to perform an iterative module cleanup to refine the module assignments in the protein correlation networks, as previously described [63]. The iterative cleanup process involved creating a bicor correlation table to assess the relationship between each protein and the respective module eigenproteins, referred to as kME. Initially, proteins with an intramodular kME below 0.30 were removed. The reassignment process consisted of reallocating proteins in the gray module (those not assigned to any module) to any module with a maximum kME greater than 0.30 and reassigning proteins whose intramodular kME was more than 0.10 below their maximum kME relative to any other module. This procedure continued iteratively until the minimum kME of the proteins in a module was above the threshold of 0.30 and the difference between the maximum kME and the intramodular kME was less than 0.1, or up to 30 iterations if module reassignment criteria were not met. After each reassignment, the module eigenproteins and the kME table were recalculated using the *moduleEigengenes* and *signedKME* functions, ensuring that all module assignments remained valid and appropriately ranked. Ultimately, this cleanup procedure reinforced the reliability of the module structure by systematically refining the assignments of proteins to their respective modules based on kME values.

After the iterative module cleanup was performed, correlations between module eigenproteins (MEs) and clinical variables (*APOE* genotype, age, Sex, co-pathologies, and Aβ and pTau levels) were calculated and plotted in a heatmap using the *labeledHeatmap* function of the WGCNA package. Subsequently, GO enrichment analysis was performed for each of the correlation networks using the function *enrichGO* from the package *clusterProfiler*, filtering GO terms to an FDR < 0.05 using the Benjamini–Hochberg method followed by the *simplify* function with a cutoff of 0.7 to remove heavily redundant terms.

Results

Amyloid-β and Tau pathologies are significantly increased in DS

AD pathology was assessed using the Braak and Thal staging or equivalent ABC score, for all cases used for proteomics analysis (Table 1, detailed case history in Supp. Table 1). Age was significantly different ($p < 0.0001$) in the LOAD cohort in comparison to the other experimental groups. However, we included eight controls ≤ 65 years old and the remaining 12 cases ≥ 65 to compensate for the age gap between EOAD and LOAD (Supp. Table 1). In addition, multiple variable linear regression analysis showed that age ($p = 0.97$) and sex ($p = 0.45$) did not contribute significantly to the differences observed in the proteomics analysis (Supp. Table 2).

Assessment of the regional distribution of Aβ and Tau pathology (Supp. Figure 1a, b) in all cases showed that Aβ levels in hippocampal and temporal regions were similar in DS and EOAD. However, Aβ quantities in DS were significantly higher ($p = 0.013$) compared to LOAD (Supp. Figure 1c). PHF-1 immunoreactive Tau pathology was significantly higher in DS compared to EOAD and LOAD ($p = 0.0002$ and $p < 0.0001$, respectively) (Supp. Figure 1d). Aβ and Tau pathology were not significantly different between EOAD and LOAD (Supp. Figure 1c–d). These results suggest an exacerbated Aβ and Tau pathology in DS despite the advanced stage of AD for all the cases in the cohorts evaluated.

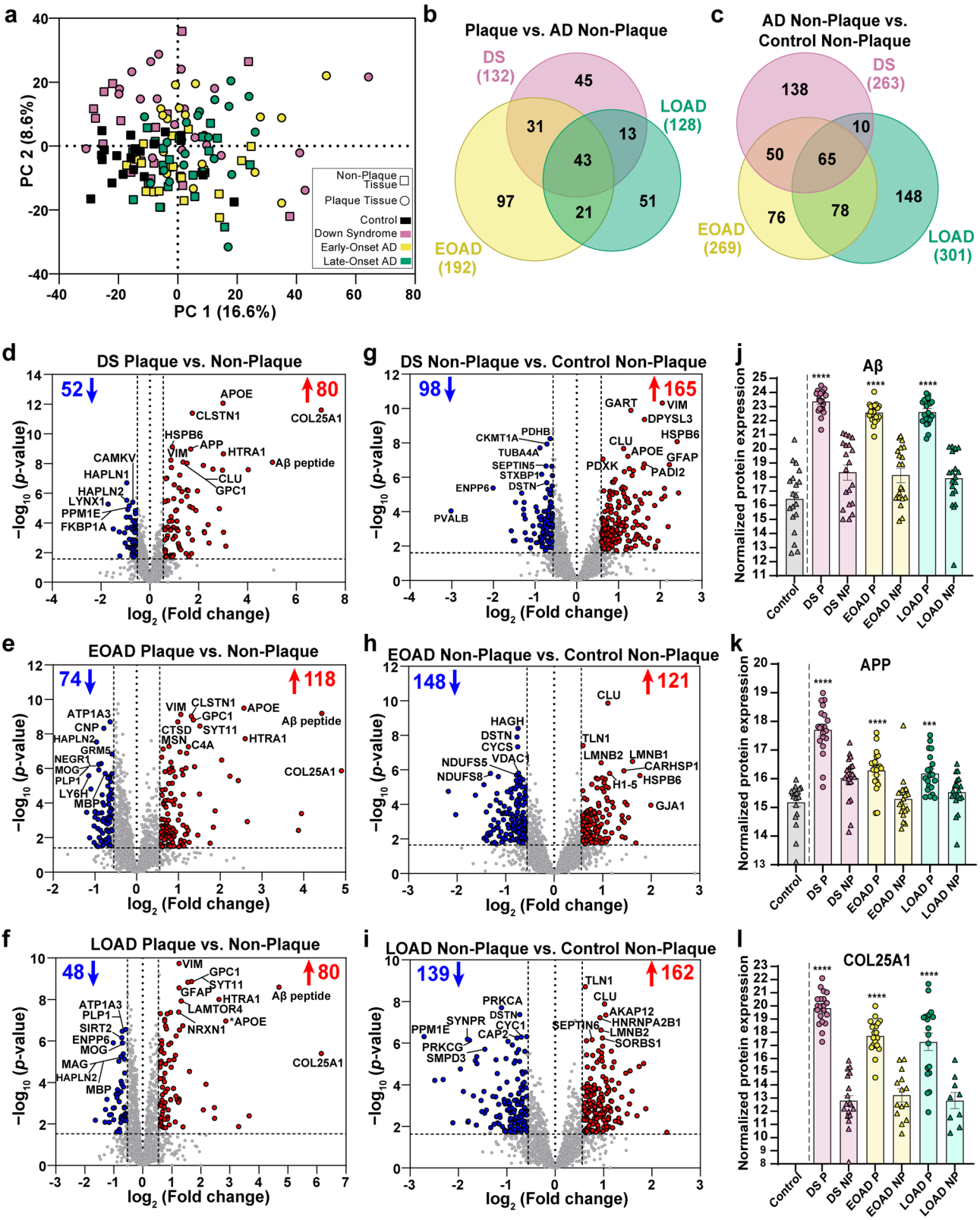
a
PC 2 (8.6%)
PC 1 (16.6%)
Non-Plaque Tissue
Plaque Tissue
Control
Down Syndrome
Early-Onset AD
Late-Onset AD
b
Plaque vs. AD Non-Plaque
DS (132)
LOAD (128)
EOAD (192)
45
31
13
43
97
21
51
c
AD Non-Plaque vs. Control Non-Plaque
DS (263)
EOAD (269)
LOAD (301)
138
10
50
65
148
76
78
d
DS Plaque vs. Non-Plaque
52
80
APOE
CLSTN1
COL25A1
HSPB6
APP
VIM
HTRA1
Aβ peptide
CAMKV
HAPLN1
CLU
GPC1
HAPLN2
LYNX1
PPM1E
FKBP1A
−log10 (p-value)
log2 (Fold change)
g
DS Non-Plaque vs. Control Non-Plaque
98
165
GART
VIM
DPYSL3
HSPB6
CKMT1A
PDHB
TUBA4A
CLU
APOE
GFAP
SEPTIN5
PDXK
PADI2
STXBP1
ENPP6
DSTN
PVALB
e
EOAD Plaque vs. Non-Plaque
74
118
ATP1A3
VIM
CLSTN1
GPC1
APOE
Aβ peptide
CNP
CTSD
SYT11
HAPLN2
MSN
HTRA1
C4A
GRM5
NEGR1
COL25A1
MOG
PLP1
LY6H
MBP
h
EOAD Non-Plaque vs. Control Non-Plaque
148
121
CLU
HAGH
DSTN
CYCS
TLN1
LMNB2
LMNB1
CARHSP1
NDUFS5
VDAC1
NDUFS8
HSPB6
H1-5
GJA1
f
LOAD Plaque vs. Non-Plaque
48
80
VIM
GPC1
SYT11
GFAP
HTRA1
Aβ peptide
ATP1A3
LAMTOR4
PLP1
*APOE
SIRT2
NRXN1
ENPP6
MOG
COL25A1
MAG
HAPLN2
MBP
i
LOAD Non-Plaque vs. Control Non-Plaque
139
162
TLN1
CLU
PRKCA
AKAP12
DSTN
SYNPR
CYC1
SEPTIN6
HNRNPA2B1
PPM1E
CAP2
LMNB2
PRKCG
SORBS1
SMPD3
j
Aβ
Normalized protein expression
Control
DS P
DS NP
EOAD P
EOAD NP
LOAD P
LOAD NP
k
APP
l
COL25A1

◂**Fig. 2** Principal component analysis (PCA) and differential protein expression in Aβ plaques and non-plaque tissue. **a** PCA shows the distribution of the $n = 20$ cases per each experimental group, with minimal segregation. **b** Venn diagram of differentially abundant Aβ plaque proteins shows 43 common proteins for all the AD subtypes evaluated, 45 for DS, 97 for EOAD, and 51 for LOAD. **c** Venn diagram of differentially abundant non-plaque proteins depicts 138 proteins in DS, 76 proteins in EOAD, 148 proteins in LOAD, and 65 common proteins for all AD subtypes. **d–f** Volcano plots indicate differentially expressed proteins (enriched in red, decreased in blue) in Aβ plaques compared to non-plaque tissue in DS (132 proteins, **d**), EOAD (192 proteins, **e**) and LOAD (128 proteins, **f**). **g–i** Volcano plots depict differentially expressed proteins in DS non-plaque tissue compared to controls (263 proteins, **g**), EOAD non-plaques (269 proteins, **h**), and LOAD non-plaques (301 proteins, **i**). **j–l** Normalized protein expression obtained from the label-free quantitative mass spectrometry proteomics of Aβ peptide (**j**), APP protein (**k**), and COL25A1 (**l**). Significance was determined using a student's two-tailed *t* test (FDR < 5%, fold-change > 1.5). *P* values are indicated based on the pairwise comparisons. *** $p < 0.001$, **** $p < 0.0001$. Error bars indicate standard error of the mean (SEM). Significant pairwise comparisons are indicated for those analyses that were performed, and controls are shown as reference

Protein abundance in amyloid plaques and non-plaque tissue varies across DS, EOAD, and LOAD

Aβ plaque pairwise comparisons

Protein differential expression in Aβ plaques and adjacent AD non-plaque tissue was evaluated using LFQ-MS in the microdissected hippocampus and temporal cortex (Fig. 1). LFQ-MS identified 1995 proteins (Supp. Tables 3–4), detected in at least 50% of the cases in any of the groups. PCA showed minimal segregation by groups (DS, EOAD, LOAD, or control) or by sample type (plaques and non-plaque tissue).

We identified 132 differentially abundant proteins in DS Aβ plaques compared to DS non-plaque tissue (Fig. 2b, d), 192 proteins in EOAD plaques vs. EOAD non-plaques (Fig. 2b, e), and 128 proteins in LOAD plaques vs. LOAD non-plaque tissue (FDR ≤ 5%, FC ≥ 1.5) (Fig. 2b, f). From these sets of proteins, 43 were shared between the three cohorts. We found 45 proteins with differential enrichment in plaques in DS, 97 proteins in EOAD, and 51 proteins in LOAD (Fig. 2b), indicating that enrichment of some proteins in Aβ plaques is variable in each experimental group. We observed a consistent enrichment of AD associated proteins such as the Aβ specific peptide LVFFAEDVGSNK (sequence corresponds to amino acids 17–28 of APP, Fig. 2d–f, j). This peptide does not discriminate between cleaved or full-length sequences. However, previous findings have shown a strong correlation to Aβ pathology [31, 49, 106]. We also identified previously detected amyloid plaque proteins, such as HTRA1, GPC1, VIM, APOE, CLSTN1, and SYT11 within the top ten most significant proteins across groups (Table 2). As expected, APP was within the top ten significantly abundant proteins in DS amyloid plaques (Fig. 2d) and was also significantly enriched in amyloid plaques in EOAD and LOAD (Fig. 2k). The plaque-protein COL25A1 [collagen alpha-1(XXV) chain, also known as CLAC-P] was the most abundant protein in amyloid plaques in all experimental groups, showing more enrichment in plaques than the Aβ peptide (Fig. 2d–f, l). Interestingly, COL25A1 was below mass spectrometry detection threshold in all control tissues (Fig. 2l), suggesting that this protein is highly correlated to Aβ plaque pathology. COL25A1 was increased 129.5-fold in DS, 29.9-fold in EOAD and 71-fold in LOAD (Table 2). In addition, COL25A1 was within the top ten significant proteins only in DS (Table 2). Hyaluronan and proteoglycan link protein 2 (HAPLN2, also known as Bral1) was within the most significant proteins decreased in plaques in the three cohorts studied. In addition, we observed decreased plaque-protein levels of oligodendrocyte proteins. MOG was significantly decreased in all groups, and MAG and MBP were significantly decreased in EOAD and LOAD amyloid plaques, respectively (Supp. Table 3). MAG and MBP levels were also decreased in plaques in DS, although it did not meet our significance criteria. The glucose transport facilitator SLC2A3 (also known as GLUT3) was decreased in amyloid plaques in all groups, yet it was significant only in EOAD and LOAD (Table 2). Overall, we observed similar proteins altered in Aβ plaques in all groups evaluated. However, most of the proteins show different abundance levels in plaques of DS, EOAD, and LOAD, accounting for the differences observed among groups.

AD non-plaque tissue pairwise comparisons

We identified 263 differentially expressed proteins in DS non-plaque tissue compared to control non-plaque tissue (Fig. 2c, g), 269 proteins in EOAD non-plaque tissue vs. control non-plaque tissue (Fig. 2c, h), and 301 significantly altered proteins in LOAD non-plaque tissue vs. control non-plaque tissue (Fig. 2c, i). We identified 65 altered non-plaque proteins compared to control tissue that were common between all cohorts evaluated (Fig. 2c). We also observed 138 proteins with differential enrichment levels in DS non-plaque tissue, 76 proteins in EOAD, and 148 proteins in LOAD (Fig. 2c). Notably, we identified among the top ten enriched proteins in DS non-plaque tissue CLU, VIM, HSPB6, and SYNM (Supp. Table 5), which we also found enriched in amyloid plaques in all disease groups. CLU was consistently enriched in non-plaque tissue in the three groups evaluated when compared to control tissue (Supp. Table 5). VIM and HSPB6 were also among the most enriched proteins in EOAD non-plaque tissue (Supp. Table 5). Conversely, we identified the actin-binding protein destrin (DSTN) as the only

Table 2 Top 20 significant proteins in Down syndrome, and early-onset and late-onset AD for 'plaque vs. non-plaque' pairwise comparisons

Down syndrome—Plaque vs Non-plaque						
Uniprot Accession ID	Gene name	Name	*p* value	Fold Change	Change in EOAD	Change in LOAD
Increased						
Q9BXS0	COL25A1	Collagen alpha-1(XXV) chain	2.51E-12	129.5	↑	↑
	Aβ		8.16E-09	32.5	↑	↑
Q92743	HTRA1	Serine protease HTRA1	2.24E-09	8.1	↑	↑
P02649	APOE	Apolipoprotein E	8.6E-13	8.0	↑	↑
O94985	CLSTN1	Calsyntenin-1	4.12E-12	3.3	↑	↑
P05067	APP	Amyloid-beta precursor protein	1.07E-09	3.2	↑	↑
P35052	GPC1	Glypican-1	9.46E-09	2.9	↑	↑
P10909	CLU	Clusterin	7.95E-09	2.6	↑	↑
O14558	HSPB6	Heat shock protein beta-6	7.59E-10	1.9	↑	↑
P08670	VIM	Vimentin	6.01E-09	1.8	↑	↑
Decreased						
P0DP58	LYNX1	Ly-6/neurotoxin-like protein 1	5.39E-06	3.3	↓	↓
P42677	RPS27	40S ribosomal protein S27	4.11E-05	1.9	↓	
Q9GZV7	HAPLN2	Hyaluronan and proteoglycan link protein 2	3E-06	1.9	↓	↓
P10915	HAPLN1	Hyaluronan and proteoglycan link protein 1	2.03E-07	1.9	↓	↓
P62942	FKBP1A	Peptidyl-prolyl cis–trans isomerase FKBP1A	1.26E-05	1.9	↓	
Q8WY54	PPM1E	Protein phosphatase 1E	7.22E-06	1.8		↓
P13987	CD59	CD59 glycoprotein	4.05E-05	1.8		↓
Q8NCB2	CAMKV	CaM kinase-like vesicle-associated protein	4.01E-06	1.6		
O75363	BCAS1	Breast carcinoma-amplified sequence 1	1.48E-05	1.5	↓	↓
Q9H9H5	MAP6D1	MAP6 domain-containing protein 1	2.36E-05	1.5	↓	
Early-onset AD—Plaque vs Non-plaque						
Uniprot Accession ID	Gene name	Name	*p* value	Fold Change	Change in DS	Change in LOAD
Increased						
	Aβ		6.43E-10	21.6	↑	↑
Q92743	HTRA1	Serine protease HTRA1	1.84E-08	6.0	↑	↑
P02649	APOE	Apolipoprotein E	3.18E-10	5.9	↑	↑
Q9BT88	SYT11	Synaptotagmin-11	3.45E-09	2.9	↑	↑
P35052	GPC1	Glypican-1	1.51E-09	2.6	↑	↑
O94985	CLSTN1	Calsyntenin-1	9.36E-10	2.5	↑	↑
P0C0L4	C4A	Complement C4-A	5.49E-08	2.4	↑	↑
P08670	VIM	Vimentin	7.4E-10	2.1	↑	↑
P07339	CTSD	Cathepsin D	1.97E-09	2.0	↑	↑
P26038	MSN	Moesin	5.16E-08	1.7		↑
Decreased						
O94772	LY6H	Lymphocyte antigen 6H	2.55E-06	2.2		↓
Q9GZV7	HAPLN2	Hyaluronan and proteoglycan link protein 2	2.88E-08	1.9	↓	↓
Q16653	MOG	Myelin-oligodendrocyte glycoprotein	5.84E-07	1.9	↓	↓
P60201	PLP1	Myelin proteolipid protein	1.18E-06	1.9	↓	↓
Q7Z3B1	NEGR1	Neuronal growth regulator 1	5.09E-07	1.8		
P09543	CNP	2',3'-cyclic-nucleotide 3'-phosphodiesterase	4.73E-09	1.7		
P02686	MBP	Myelin basic protein	1.97E-06	1.7		↓

Table 2 (continued)

Early-onset AD—Plaque vs Non-plaque						
Uniprot Accession ID	Gene name	Name	*p* value	Fold Change	Change in DS	Change in LOAD
P13637	ATP1A3	Sodium/potassium-transporting ATPase subunit alpha-3	1.95E-09	1.6		↓
P11169	SLC2A3	Solute carrier family 2, facilitated glucose transporter member 3	1.97E-06	1.5		↓
P41594	GRM5	Metabotropic glutamate receptor 5	1.45E-07	1.5		↓
Late-onset AD—Plaque vs Non-plaque						
Uniprot Accession ID	Gene name	Name	*p* value	Fold change	Change in DS	Change in EOAD
Increased						
	Aβ		2.55E-09	25.8	↑	↑
Q92743	HTRA1	Serine protease HTRA1	9.94E-09	6.2	↑	↑
P35052	GPC1	Glypican-1	1.39E-09	3.2	↑	↑
Q9BT88	SYT11	Synaptotagmin-11	1.5E-09	2.9	↑	↑
Q0VGL1	LAMTOR4	Regulator complex protein LAMTOR4	1.19E-08	2.5	↑	↑
P14136	GFAP	Glial fibrillary acidic protein	2.78E-09	2.4		↑
P08670	VIM	Vimentin	1.87E-10	2.4	↑	↑
Q9ULB1	NRXN1	Neurexin-1	4.05E-08	2.4	↑	↑
Q9UM22	EPDR1	Mammalian ependymin-related protein 1	4.23E-08	1.9	↑	↑
P55084	HADHB	Trifunctional enzyme subunit beta, mitochondrial	4.83E-08	1.5		
Decreased						
Q6UWR7	ENPP6	Glycerophosphocholine cholinephosphodiesterase ENPP6	1.23E-06	2.0	↓	↓
O75363	BCAS1	Breast carcinoma-amplified sequence 1	9.47E-06	1.8	↓	↓
Q9GZV7	HAPLN2	Hyaluronan and proteoglycan link protein 2	5.75E-06	1.7	↓	↓
Q8IXJ6	SIRT2	NAD-dependent protein deacetylase sirtuin-2	7.07E-07	1.7		↓
P60201	PLP1	Myelin proteolipid protein	3.38E-07	1.6	↓	↓
Q16653	MOG	Myelin-oligodendrocyte glycoprotein	1.25E-06	1.6	↓	↓
P20916	MAG	Myelin-associated glycoprotein	4.16E-06	1.6		↓
P02686	MBP	Myelin basic protein	7.42E-06	1.6		↓
P11169	SLC2A3	Solute carrier family 2, facilitated glucose transporter member 3	3.52E-05	1.5		↓
P13637	ATP1A3	Sodium/potassium-transporting ATPase subunit alpha-3	2.8E-07	1.5		↓

protein among the top ten significantly decreased proteins in non-plaque tissue from DS, EOAD, and LOAD cohorts compared to controls (Supp. Table 5). We also observed that parvalbumin (PVALB) was the most decreased protein in DS non-plaque tissue compared with controls (Fig. 2g), whereas the levels of PVALB in EOAD and LOAD were not significantly different from controls (Supp. Table 4). Our proteomics findings in non-plaque tissue showed that there were more differences in protein levels in non-plaque tissue between groups, in comparison to the more consistent protein levels in plaques, highlighting the largely similar plaque proteome between AD subtypes despite differences in baseline, non-plaque-protein expression.

Amyloid plaque proteomes of DS, EOAD, and LOAD are highly correlated

We performed correlation analyses to compare the proteomes of Aβ plaques and non-plaque tissues in DS, EOAD, and LOAD. Proteins included in the correlations were significant and FC > 1.5 at least in one of the groups evaluated. For amyloid plaques, there was a positive correlation between

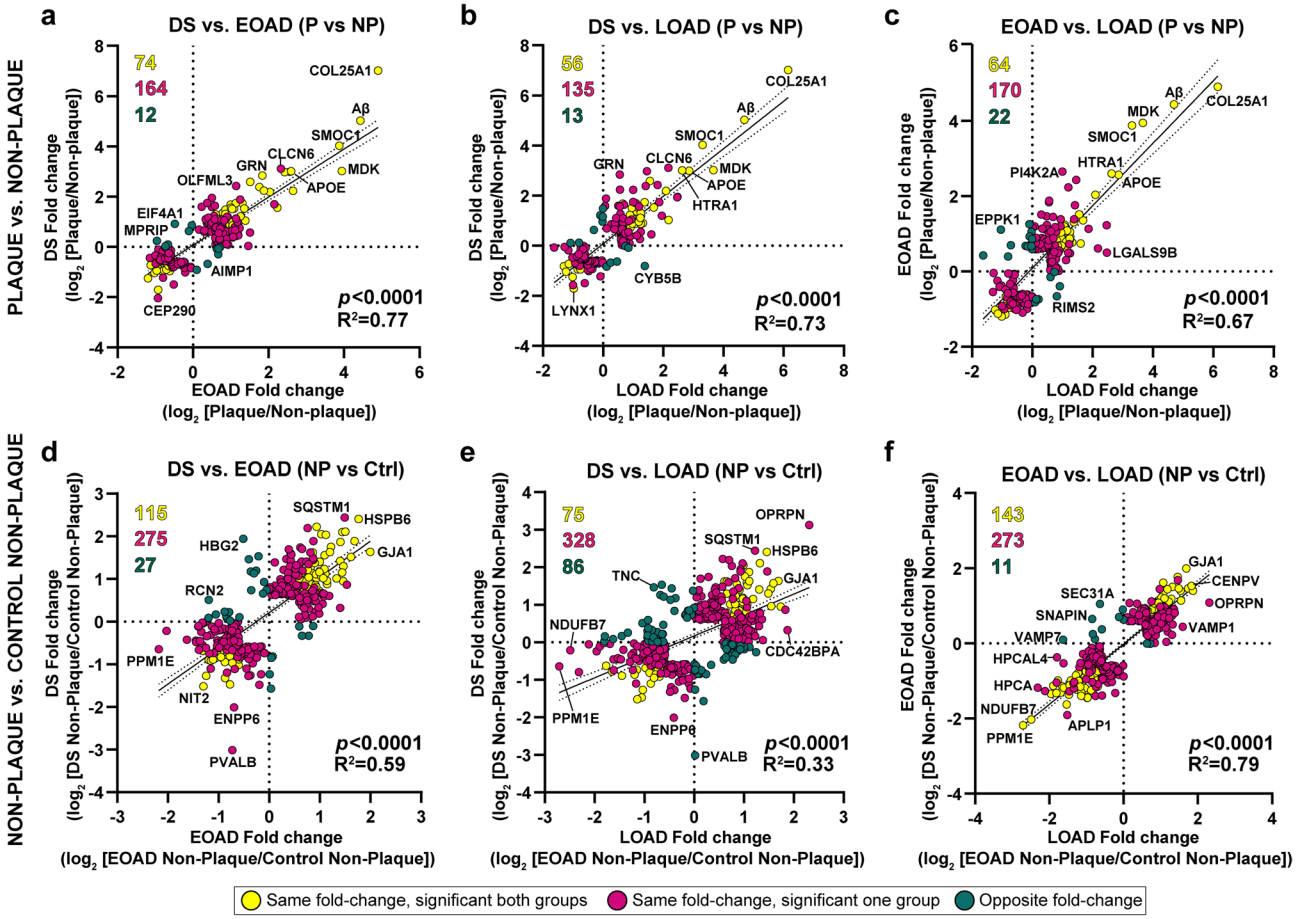

Fig. 3 Correlation analyses of differentially abundant proteins in Aβ plaques and non-plaque tissue. **a–c** Correlation analyses for significant proteins in Aβ plaques vs non-plaque tissue and **d–f** DS, EOAD and LOAD non-plaque vs control non-plaque tissue. Yellow dots represent proteins changing in the same direction (highly abundant or less abundant proteins in both groups evaluated) and that are significant for both groups compared. Magenta dots represent proteins changing in the same direction, but are significant only in one of the groups evaluated. Green dots represent proteins changing in opposite direction (i.e., abundant in one group and less abundant in the other group evaluated). Numbers are colored to match the dots. Proteins were selected for the correlation analysis if they were significant at least in one of the groups compared and its fold-change > 1.5. We observed a positive correlation between DS vs. EOAD **a** ($p < 0.0001$, $R^2 = 0.77$, **b** DS vs. LOAD ($p < 0.0001$, $R^2 = 0.73$) and **c** EOAD vs. LOAD ($p < 0.0001$, $R^2 = 0.67$). There is also a positive correlation when comparing non-plaque proteins in **d** DS vs. EOAD ($p < 0.0001$, $R^2 = 0.59$) and **e** DS vs. LOAD ($p < 0.0001$, $R^2 = 0.33$). **h.** Correlation between EOAD and LOAD non-plaque proteins ($p < 0.0001$, $R^2 = 0.79$)

DS and EOAD ($R^2 = 0.77$, $p < 0.0001$). We observed 65.5% (164/250) of the proteins changing in the same direction (i.e., fold-change for a protein is positive or negative in both groups), where 29.6% (74/250) of the proteins were significantly altered in DS and EOAD plaques (Fig. 3a). We only observed 4.8% (12/250) of the proteins changing in different directions (i.e., fold-change for a protein is positive in one group and negative in the other) (Fig. 3a). DS and LOAD plaque proteomes also correlated positively ($R^2 = 0.73$, $p < 0.0001$), with 66.2% (135/204) of the proteins with same fold-change direction and 27.5% (56/204) of the proteins significantly altered in both groups (Fig. 3b). Similar to DS and EOAD, only 6.3% (13/204) of the proteins were changing in opposite direction (Fig. 3b). There was also a positive correlation between EOAD and LOAD differentially abundant plaque proteins ($R^2 = 0.67$, $p < 0.0001$), similar to what we observed between DS vs. the AD subtypes evaluated. We identified 66.4% (234/256) of the proteins changing in the same direction, and 25% (64/256) of the proteins were significant in both groups (Fig. 3c). The proteins changing in opposite direction accounted for 8.6% (22/256) of the total (Fig. 3c). Our analysis shows high similarity among the proteins altered in Aβ plaques vs. non-plaques of DS, EOAD, and LOAD, with the majority of the proteins changing in the same direction.

Correlation analyses of DS, EOAD, and LOAD non-plaque differentially abundant proteins showed positive correlations between DS and EOAD ($R^2 = 0.59$, $p < 0.0001$)

and a weaker correlation between DS and LOAD ($R^2 = 0.33$, $p < 0.0001$) (Fig. 3d–e). We observed 65.9% (275/417) of the proteins changing in the same direction in DS and EOAD Aβ plaques, where 27.6% (115/417) of the proteins were significantly altered in both groups. We observed 6.5% (27/417) of proteins changing in the opposite direction (Fig. 3d). Similarly, 67.1% (328/489) of the proteins in DS and LOAD were changing in the same direction (Fig. 3e). We observed that 15.3% (75/489) of the proteins were significant in both groups, whereas 17.6% (86/489) of proteins had opposite fold changes (Fig. 3e). Moreover, we observed a higher positive correlation between EOAD vs. LOAD non-plaque proteomes ($R^2 = 0.79$, $p < 0.0001$), with 63.9% (273/427) of the proteins were changing in the same direction, with 33.5% (143/427) being also significant in both groups (Fig. 3f). Only 2.6% (11/427) of the proteins were changing in opposite directions (Fig. 3f). Overall, we observed a similar 'amyloid plaques protein signature' across the experimental groups. Nonetheless, correlations of the non-plaque tissue proteomes suggest a higher similarity between EOAD and LOAD differentially enriched proteins in comparison to DS.

Protein-coding genes present in Hsa21 are not associated with protein enrichment in Aβ plaques

We performed chromosomal mapping of significantly altered proteins identified through proteomic analysis across all human chromosomes using the UCSC Human Genome Browser to evaluate the distribution of these proteins across DS, EOAD, and LOAD. Supplemental Figure 2 illustrates the percentage of significantly altered proteins for each group. The overall percentage of proteins from each chromosome was below 20%, and no single chromosome exhibited a markedly overrepresented protein expression pattern. This suggests that proteins from all chromosomes, not just Hsa21, contribute to the molecular differences observed in both DS and AD.

Of the 1995 proteins identified in this study, 22 were from Hsa21 (Fig. 4). We compared these proteins with those reported in a previous DS plaque proteomics study [31], identifying a total of 26 Hsa21 proteins between the two studies. A significant portion, 69.2% (18/26), of these proteins were shared between the current and previous studies (Fig. 4). Among the proteins identified, APP was significantly altered in Aβ plaques in all cohorts (Fig. 4). GART was significantly abundant in LOAD and DS non-plaque tissue (Fig. 4a, c), and PCP4 was differentially expressed in LOAD and EOAD non-plaque tissue (Fig. 4a, b). CXADR was differentially expressed in EOAD amyloid plaques (Fig. 4b). APP was also significantly enriched in DS non-plaque tissue (FDR < 0.05, Fig. 4a). NCAM2, CBR1, CBR3, PDXK, CSTB, and COL6A1 were

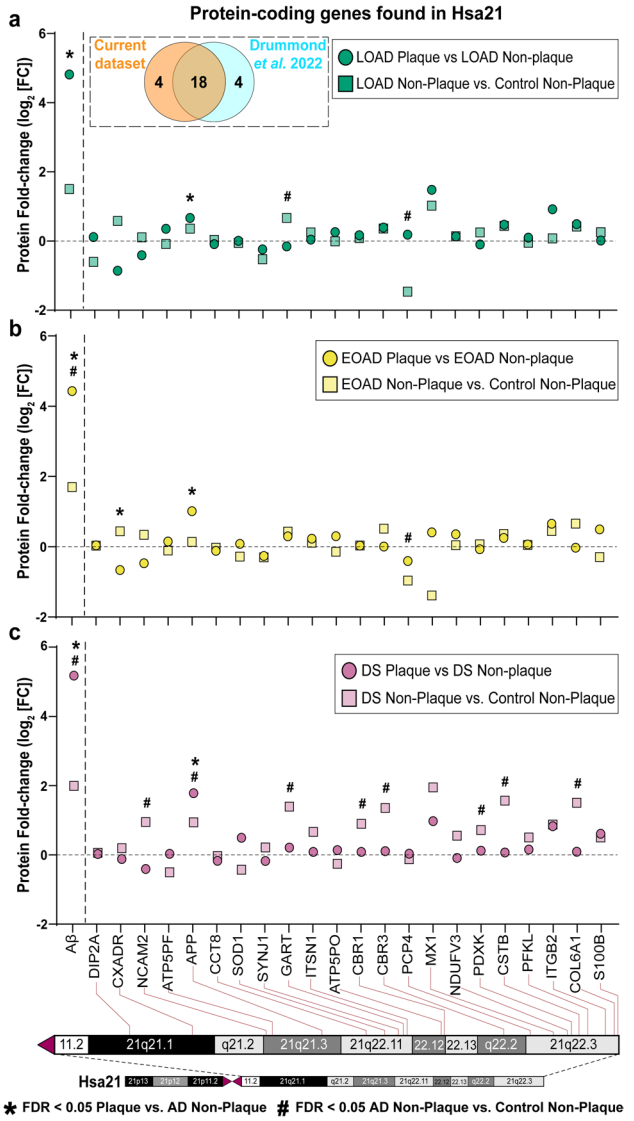

Fig. 4 Mapping protein-coding genes to chromosome 21 (Hsa21). **a** Dashed box contains Venn diagram of proteins from genes in Hsa21 identified in the current study vs. Drummond et al. 2022, [31]. **a–c** The figure depicts fold-change (Log_2 FC) of the 22 Hsa21 genes whose corresponding protein products were found in Aβ plaques (circles) or neighboring non-plaque tissue (squares) in LOAD (**a**) EOAD (**b**) and DS (**c**). Paired two-tailed *t* tests (plaques vs. non-plaques) or unpaired two-tailed *t* tests (non-plaques vs. control) with permutation correction at a 5% FDR are indicated. Aβ peptide is shown as reference

significantly enriched in DS non-plaque tissue (Fig. 4a). Taken together, these results along with the chromosomal mapping of all significantly altered proteins suggest that Hsa21 triplication does not necessarily lead to the enrichment of those gene products in Aβ plaques or in the surrounding non-plaque tissue.

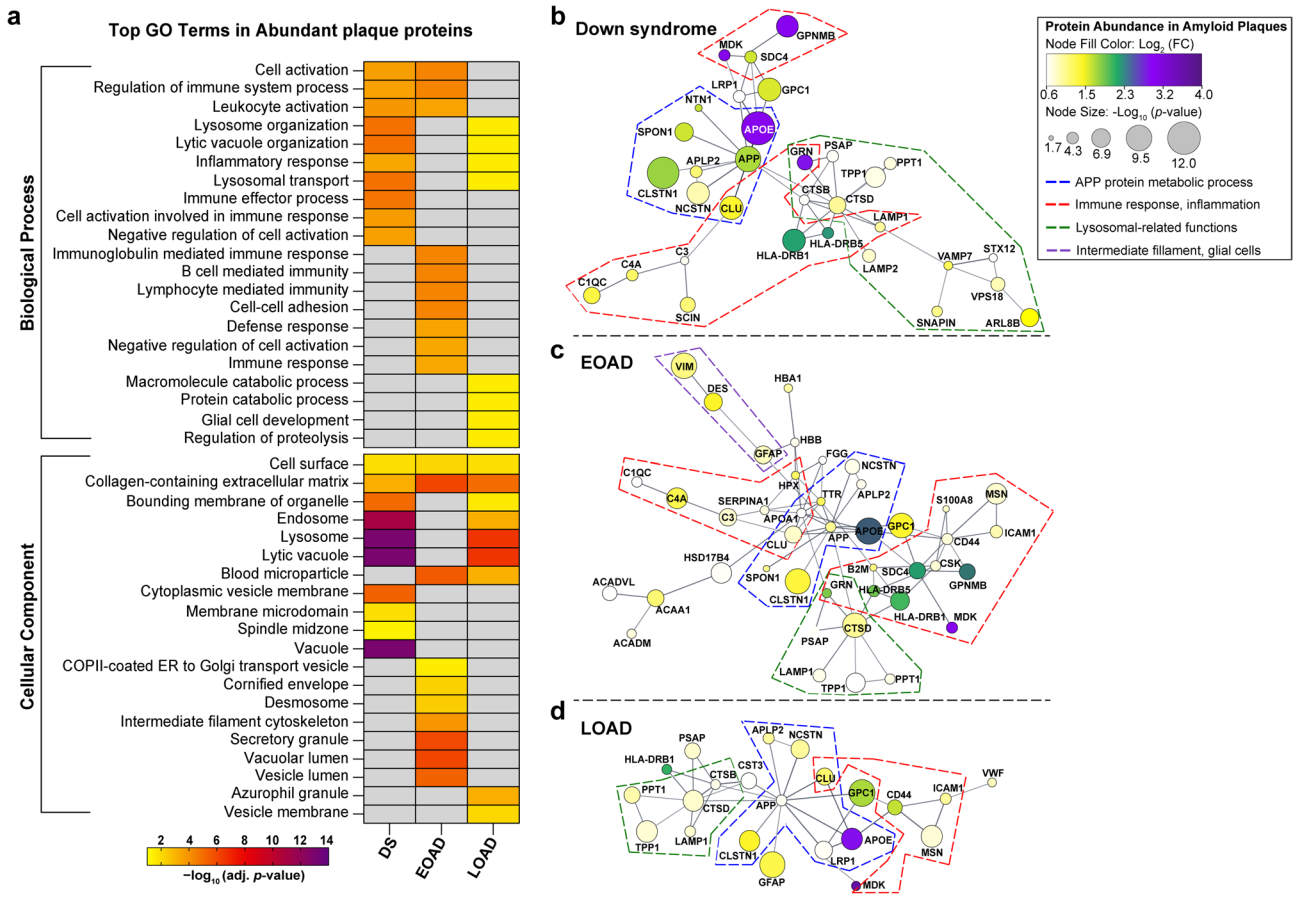

Fig. 5 Gene ontology annotation and protein–protein interaction networks of significantly abundant proteins in Aβ plaques. **a** GO terms heatmap depicts top ten enriched BP and CC GO terms for significantly abundant Aβ plaque proteins in DS, EOAD, and LOAD. Color indicates the adjusted p value < 0.05 (− Log_{10} [adj. p value]). **b–d** Protein networks (PPI Enrichment $p = 1 \times 10^{-16}$) show functional and physical amyloid plaques protein associations in DS (**b**), EOAD (**c**) and LOAD (**d**). Node color indicates fold-change ($\log_2$ [FC]) and node size depicts adjusted p value (-$\log_{10}$ [p value]) from the student's two-tailed t test. Disconnected nodes are not shown in the network. Colored dotted lines highlight groups of proteins based on functions/pathways observed in the GO terms; blue: APP protein metabolic process, red: immune response and inflammation, green: lysosomal-related functions, and purple: intermediate filament proteins, glial cells. GO terms annotation was performed using R package *clusterProfiler* v 4.8.2. PPI networks were created in Cytoscape v 3.10.0 using STRING database v 11.5

Aβ plaque-protein signature is related to APP processing, immunity, and lysosomes

Aβ plaques functional analyses

We identified functional associations for the significantly abundant proteins in Aβ plaques and AD non-plaque tissue by performing 'GO enrichment analysis' (FDR < 0.05, Supp. Tables 6–13). Top enriched biological process (BP) GO terms in DS included lytic vacuole organization, lysosome organization, and lysosomal transport (for the three terms, $p = 1.29 \times 10^{-5}$, Fig. 5a, Supp. Table 6). We also identified terms cell activation ($p = 0.00024$), regulation of immune system process ($p = 0.00027$), and leukocyte activation ($p = 0.00016$), which were also observed in EOAD (Fig. 5a). For cellular component (CC), we identified as the top terms vacuole, lysosome, lytic vacuole ($p = 9.56 \times 10^{-14}$), and endosome ($p = 9.71 \times 10^{-14}$, Fig. 5a, Supp. Table 10), similarly as BP GO terms. In contrast, EOAD most enriched BP terms were regulation of immune system process, B-cell-mediated immunity, immunoglobulin-mediated immune response, and lymphocyte-mediated immunity ($p = 4.33 \times 10^{-5}$, Fig. 5a, Supp. Table 6). Top CC GO terms in EOAD were secretory granule ($p = 1.13 \times 10^{-6}$), vacuolar lumen, and collagen-containing extracellular matrix (both $p = 8.75 \times 10^{-7}$, Fig. 5a, Supp. Table 10). LOAD also showed BP GO terms related to lysosomes as observed in DS, yet with a lower significance. For instance, we identified lysosomal transport and organization and lytic vacuole organization ($p = 0.0288$ Fig. 5a, Supp. Table 6). CC GO terms included lysosome and lytic vacuoles ($p = 2.47 \times 10^{-7}$), collagen-containing extracellular matrix ($p = 9.41 \times 10^{-6}$),

and endosome ($p = 0.00063$) (Fig. 5a, Supp. Table 10), highlighting functional similarities of plaque-associated proteins between DS and LOAD.

We also evaluated the physical and functional protein interactions of significantly abundant proteins in Aβ plaques, using Cytoscape and the STRING database (Fig. 5b–d). The networks for amyloid plaque proteins for all the cohorts evaluated showed a significant degree of protein–protein interactions (PPI enrichment $p = 1 \times 10^{-16}$). We observed a consistent group of proteins in all forms of AD evaluated, which were grouped based on functional enrichment (Fig. 5b–d). For instance, we identified proteins related to APP and Aβ metabolism (APP, APOE, CLU, CLSTN1, NCSTN, APLP2, and SPON1), immune response and inflammation (HLA-DRB1, HLA-DRB5, C1QC, C4A, and C3 consistent in DS and EOAD; CD44, ICAM1, and MSN in EOAD and LOAD), and lysosomal-related functions (PPT1, TPP1, LAMP1, PSAP, and CTSD). APOE was highly abundant in Aβ plaques in DS and LOAD (Fig. 5b, d) compared to EOAD, being the most significant in DS (Fig. 5b) in comparison to EOAD and LOAD. We also identified a group of glial-related proteins in EOAD network, namely VIM, DES, and GFAP (Fig. 5c). Overall, our findings suggest a similar plaque-protein signature in the three groups, which were functionally associated mainly to APP and Aβ processing, immunity-related responses, and lysosomal functions.

In addition, an analysis of the ten most abundant proteins (ranked by FC) differentially enriched in Aβ plaques in DS, EOAD, or LOAD further showed the relationship of Aβ plaque-associated proteins with lysosomal and immune-related functions (Supp. Table 14). According to the GO annotation, we found that the significantly enriched amyloid plaque proteins in DS predominantly relate to endo/lysosomal functions, including CLCN6, ATG9A, and VAMP7 (Fig. 6, Supp. Table 14). Oligodendrocyte protein MOG was significantly decreased in plaques for all cohorts, but

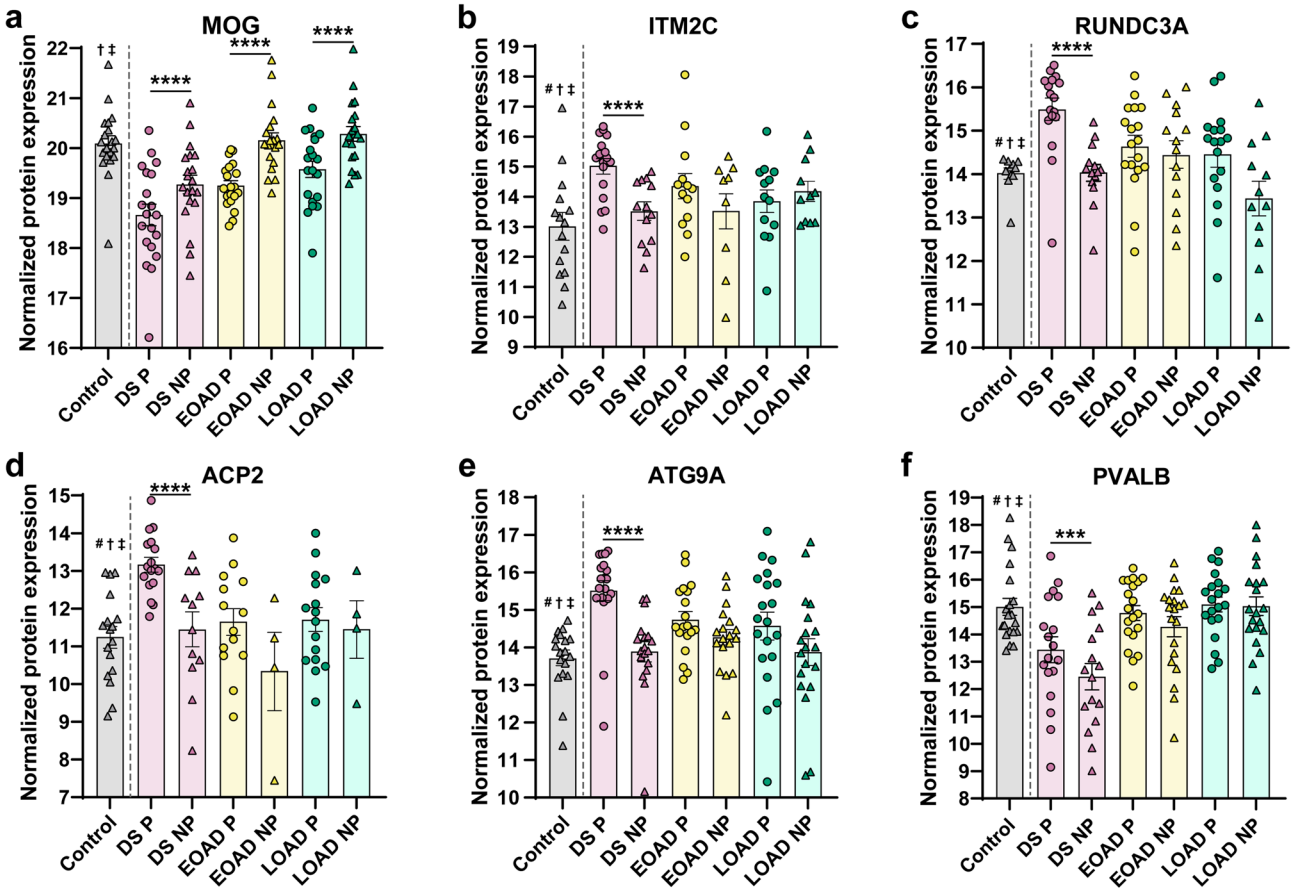

Fig. 6 Enriched Aβ plaque proteins of interest in DS compared with EOAD and LOAD. (**a–f**) Normalized protein expression obtained from the label-free quantitative mass spectrometry proteomics of abundant Aβ plaque proteins of interest in DS. Proteins are shown by order of decreasing significance. Proteins of interest were defined as significant (FDR < 5%, fold-change > 1.5) only in DS and also have known or predicted roles in AD and DS. Pairwise comparisons p values are indicated. * $p < 0.05$, **** $p < 0.0001$. Error bars indicate standard error of the mean (SEM). Significant pairwise comparisons are indicated for those analyses that were performed, controls are shown as reference. Additional symbols on top of the control bar indicate that the given protein is not significantly abundant in non-plaque AD tissue compared to controls in # DS, † EOAD, and ‡ LOAD, respectively

fold-change suggests an increased reduction in DS (Supp. Table 3, Fig. 6a) in comparison to the other groups. We identified protein ITM2C, which is involved in Aβ peptide production [29] (Fig. 6b). We also observed proteins with functions linked to presynaptic signaling and axon guidance, namely, RUNDC3A and NTN1 [60, 104] (Fig. 6). The calcium-binding protein and marker of inhibitory neurons PVALB was significantly enriched in DS plaques but was unaltered in EOAD and LOAD (Fig. 6f). In contrast, we observed that Aβ plaque proteins significantly abundant in EOAD are mostly related to immune response, immunoglobulin-mediated immune response (S100A7, HPX, and IL36G), as well as vacuole lumen and secretory vesicles related (GGH, TTR). The protein EPPK1 is linked to cytoskeletal organization functions such epithelial cell proliferation and intermediate filament organization (Supp. Table 14). In LOAD, we observed a series of proteins involved in bounding membrane of organelle, collagen-containing extracellular matrix, and vesicle membrane (CYB5B, VWF and PTPRN2). Although we did not observe particular association with GO terms, other amyloid plaque LOAD proteins, including TIMM8A, ACSS3, and SFXN5 (linked to mitochondrial functions) [89, 133, 138], THUMPD1 and RPS7 (related to RNA-binding activity and ribosomes) [14, 128] and NRXN2 (protein–protein interactions at the synapses) [76] were identified (Supp. Table 14). These observations support our findings in the GO functional enrichment and protein interaction networks, providing evidence that some of the most abundant proteins in DS plaques are primarily linked to lysosomal pathways.

Non-plaque tissue functional analyses

GO terms for abundant non-plaque proteins showed chromatin remodeling as the top BP term for all experimental groups (DS $p = 0.00128$, EOAD $p = 5.79 \times 10^{-9}$, LOAD $p = 1.69 \times 10^{-10}$, Supp. Figure 3a, Supp. Table 8). Importantly, top BP GO terms in DS were associated with integrin-mediated signaling, extracellular structure, and extracellular matrix organization ($p = 0.00684$, Supp. Figure 3a, Supp. Table 8). In contrast, EOAD and LOAD top BP GO terms included protein–DNA complex assembly ($p = 4.74 \times 10^{-6}$ and $p = 1.14 \times 10^{-8}$, respectively), regulation of gene expression (EOAD $p = 5.08 \times 10^{-5}$, LOAD $p = 1.68 \times 10^{-8}$), and nucleosome assembly (EOAD $p = 4.74 \times 10^{-6}$, LOAD $p = 3.25 \times 10^{-8}$) (Supp. Figure 3a, Supp. Table 8). Top CC GO terms for DS were collagen-containing extracellular matrix, which was also observed in EOAD and LOAD, external encapsulating structure, and extracellular matrix ($p = 3.52 \times 10^{-8}$, Supp. Figure 3a, Supp. Table 12). Top CC GO term for EOAD was nucleosome ($p = 4.44 \times 10^{-6}$), which was also identified in DS and LOAD. Other EOAD top CC GO terms were DNA packaging complex ($p = 8.01 \times 10^{-6}$) and protein–DNA complex ($p = 2.23 \times 10^{-5}$) (Supp. Figure 3a, Supp. Table 12). In a similar fashion, LOAD top CC GO terms were DNA packaging complex, protein–DNA complex (both $p = 3.78 \times 10^{-14}$), and nucleosome ($p = 1.71 \times 10^{-12}$) (Supp. Figure 3a, Supp. Table 12).

We also created protein interaction networks of non-plaque tissue DS, EOAD, and LOAD proteomes, which showed a highly significant degree of protein–protein interactions (PPI enrichment $p = 1 \times 10^{-16}$, Supp. Figure 3b–d). We observed groups of RNA-binding proteins, such as SRSF4, eukaryotic initiation factors (eIF4), and the heterogeneous nuclear ribonucleoproteins (hnRNP) protein family, primarily in EOAD and LOAD networks (Supp. Figure 3c, d). We also observed a set of intermediate filament and glial proteins, such as GFAP, AQP4, DES, VIM, ALDH1L1, and GART (Supp. Figure 3b–d). Additionally, there were groups of histone proteins related to the nucleosome, such as H2A, H2B, and H1 protein families (Supp. Figure 3b–d). Particularly, the DS protein interaction network exhibited a set of collagens, laminins, cell adhesion proteins, proteoglycans, and heparin sulfate proteins (Supp. Figure 3b) as well as proteasome and chaperone proteins also involved in regulation of gene expression, including SQSTM1, PSMB4, PSMD4, and HSPB6 (Supp. Figure 3b). Our findings highlight a pivotal role of extracellular matrix (ECM) and structural components in DS besides the proteins associated to Aβ plaque pathology.

Comparative analysis with previous human AD proteomics and identification of novel plaque proteins

We compared the differentially abundant proteins found in Aβ plaques and AD non-plaque tissue with previous human AD proteomics studies compiled in the NeuroPro database [4]. We observed that 77.7% of altered proteins identified in amyloid plaques in our study were also identified in previous AD plaque proteomics studies (Fig. 7a). From the 301 significantly altered plaque proteins that we identified in the present study, 13.6% have not been found in previous plaque proteomics studies, but only reported as significantly altered in bulk brain tissue proteomics studies (Fig. 7a). Similarly, 85.2% of the proteins we identified in the non-plaque tissue have been described in previous plaque and bulk tissue proteomics studies, whereas 10.9% have been identified in bulk human brain tissue but not in plaque proteomics studies (Fig. 7a). Interestingly, we identified in our study 34 proteins that have not been described previously in any human AD proteomics study, either in plaques or in bulk tissue (Fig. 7a, Supp. Table 15–16).

In DS specifically, we identified seven amyloid plaque proteins and eight non-plaque tissue proteins significantly

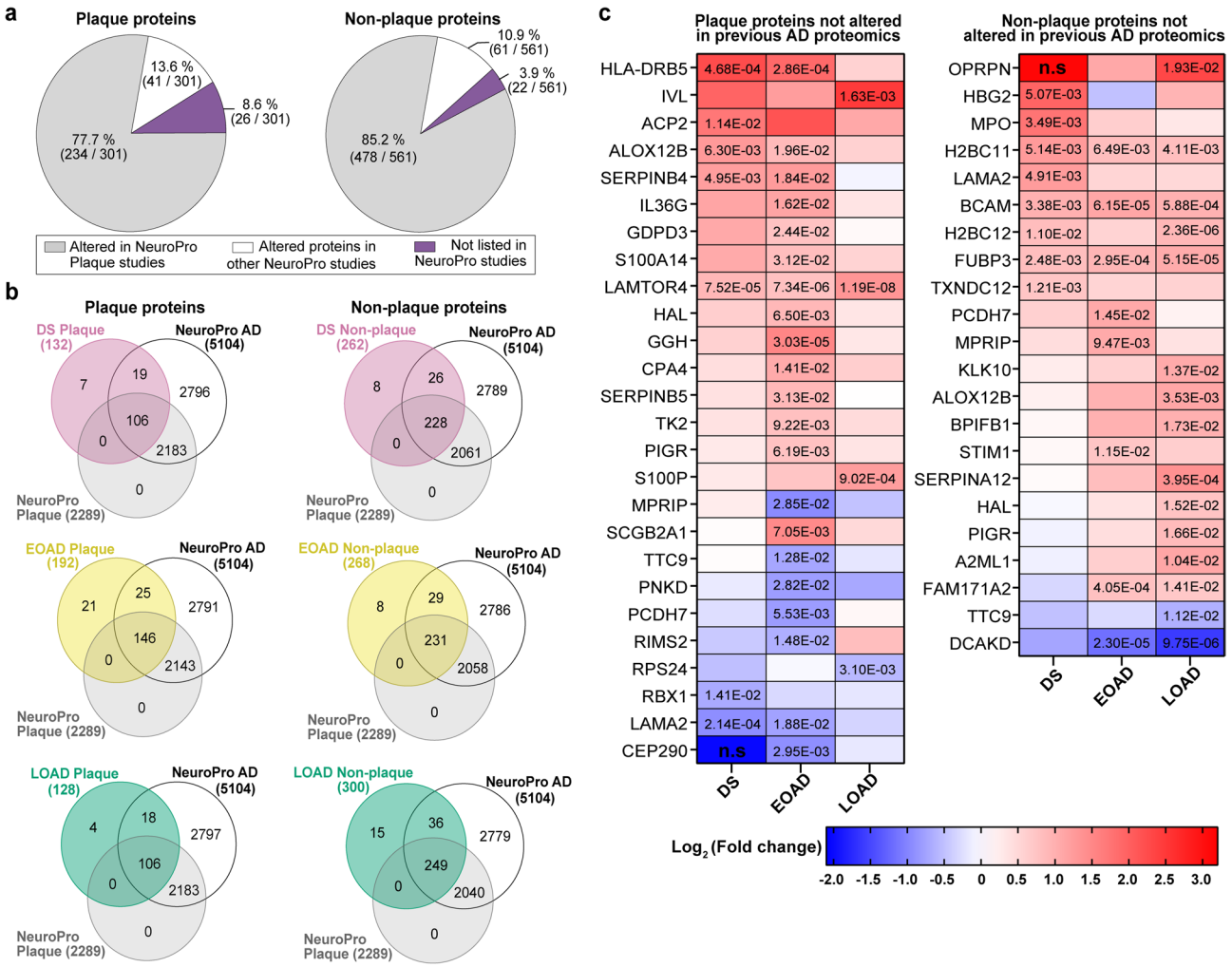

Fig. 7 Comparison of protein changes with previous advanced AD proteomics studies. **a** Altered proteins identified in the current study were compared with proteins found altered in previous AD proteomics compiled in NeuroPro [4] (v1.12; https://neuropro.biomedical.hosting/). Pie charts show that 77.7% (234/301) of altered plaque proteins in the present study have been identified in previous AD plaque proteomics studies (gray). 13.6% (41/301) of the proteins have been seen only in bulk tissue proteomics studies (white), and 8.6% (26/301) of the altered proteins observed in the current study have not been described in previous AD proteomics (purple). In a similar fashion, 85.2% (478/561) proteins altered in AD non-plaque tissue have been observed in AD plaque proteomics, 10.9% (61/561) only in bulk tissue proteomics, and 3.9% (22/561) have not been described in previous AD proteomics studies. **b** Venn diagrams illustrate the altered proteins identified in Aβ plaques and AD non-plaque tissue for each AD subtype evaluated, in comparison to the 5104 altered proteins in advanced AD registered in NeuroPro database. **c** Heatmaps depicting the fold-change (Log_2 [FC]) of the plaque and AD non-plaque altered proteins identified in the present study that have not been described in previous AD proteomics. Numbers in the cells represent the significance (FDR < 0.05) values observed in the pairwise comparisons, n.s represent no significant differences regardless of the fold-change

altered in our study, which have not been found in past AD brain tissue proteomics studies (Fig. 7b, Supp. Table 17). Similarly, we identified in EOAD 21 significantly altered proteins in plaque and eight in non-plaque tissue, which have not been described previously (Fig. 7b, Supp. Table 17). In the case of LOAD, we observed four significantly altered proteins in amyloid plaques and 15 in non-plaque tissue that have not been identified in previous AD plaques or bulk brain tissue proteomics studies (Fig. 7b, Supp. Table 17). From this group of proteins, LAMTOR4 (late endosomal/lysosomal adaptor and MAPK and MTOR activator 4) was significantly enriched in Aβ plaques in all the cohorts analyzed (Fig. 7c). The proteins HLA-DRB5, ALOX12B, and SERPINB4 were significantly enriched in DS and EOAD amyloid plaques (Fig. 7c). In contrast, LAMA2 was significantly decreased in DS and EOAD amyloid plaques (Fig. 7c). On the other hand, we observed the histone protein H2BC11, the basal cell adhesion protein BCAM, and the DNA-binding protein FUBP3 significantly enriched in non-plaque tissue in DS, EOAD, and LOAD (Fig. 7c). The protein centrosomal protein of 290 kDa (CEP290) showed a marked decrease in DS Aβ plaques compared

to DS non-plaque tissue; however, it was detected in few cases of the 20 evaluated in that cohort (Supp. Table. 3), reason why it did not reach FDR < 0.05 (Fig. 7c). The protein FAM171A2 was significantly enriched only in EOAD and LOAD, contrary to the protein DCAKD that was significantly decreased in EOAD and LOAD non-plaque tissue (Fig. 7c). Overall, our proteomics findings are consistent with previous proteomics studies. Notably, our comparative analysis allowed us to identify novel proteins in AD human proteomics.

Validation of the Aβ plaques protein signature in DS and novel plaque proteins in human DS proteomics

The NeuroPro database is a powerful tool to investigate proteomic changes in AD human brains. However, by the time of writing this article, the database does not include DS proteomics data. Therefore, we compared our DS amyloid plaques proteomics findings with our previous study (Drummond et al., 2022 [31]) where unbiased localized proteomics was used to interrogate the DS amyloid plaques proteome. In the study led by Drummond and colleagues, any Aβ plaque detected by IHC was sampled regardless of plaque morphology. We observed 2522 proteins between both DS plaque proteomics datasets, comprised of 1981 proteins in the present study and 2258 proteins in our previous work (excluding isoforms). We observed 68.1% (1717/2522) of proteins overlapping between both studies, with a total of 228 significantly altered plaque proteins in either dataset. Among these, 21.9% (50/228) were common to both studies (Fig. 8a). Particularly, 36% (82/228) of the significantly altered proteins in the present study were not significant in Drummond et al., and conversely, 42.1% (96/228) of the proteins identified in the previous study were not detected in the current dataset (Fig. 8a, Supp. Table 18). This variance may reflect differences in statistical thresholds and increased sample size, providing higher power in this study to identify more plaque-enriched proteins in DS with greater confidence. For instance, 35 proteins that were significantly enriched proteins detected in the Drummond study but not significant in ours were nonetheless observed in our dataset, with many showing increased abundance trends that nearly reached significance. In addition, from the proteins that were different between both studies (Fig. 8a), only 12 had a different direction of change, suggesting that most of the differences observed between the datasets are due to the differential stringency applied and the number of samples. Despite these differences, we observed a significant positive correlation between the Aβ plaque proteomes of the DS cohorts ($p < 0.0001$, $R^2 = 0.60$, Fig. 8b). In fact, the 50 common proteins between both studies were changing in the same direction (48 enriched and 2 decreased in plaques, Fig. 8b). Within these set of amyloid plaque

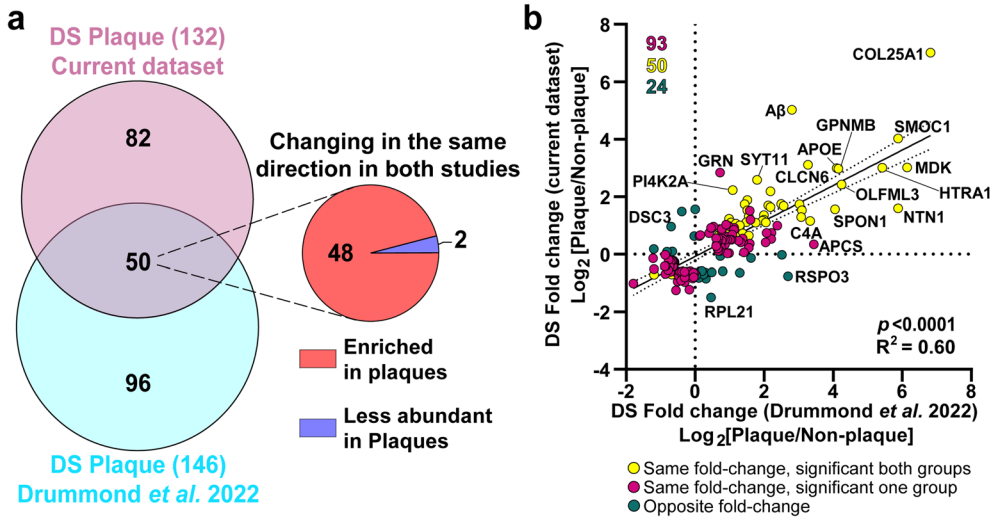

Fig. 8 Comparison of protein changes between the DS plaques localized proteomics studies. **a** Venn diagram depicts differentially abundant proteins identified in the current study and the previous DS plaque proteomics study (Drummond et al. 2022, [31]). We identified 132 significantly altered proteins compared to 146 identified previously. From the 50 common proteins identified, 48 were enriched in Aβ plaques and 2 proteins were less abundant in both studies. **b** Correlation analysis between differentially abundant proteins in the current study and previous DS localized proteomics. Yellow dots represent significant proteins changing in the same direction (highly abundant or less abundant proteins in both groups evaluated) in both groups compared. Magenta dots represent proteins changing in the same direction, but are significant only in one of the groups evaluated. Green dots represent proteins changing in opposite direction (i.e., abundant in one group and less abundant in the other group evaluated). There was a significant positive correlation ($p < 0.0001$, $R^2 = 0.60$) between the two datasets

proteins, we identified Aβ peptide, APP, COL25A1, and a set of previously described plaque proteins, such as APOE, SMOC1, CLU, C3, and CLCN6 among others (extended data in Supp. Table 18), thus validating a plaque-protein signature also observed in DS Aβ pathology. Interestingly, from the seven novel DS plaque proteins regarding the NeuroPro database (Supp. Table 17), only ACP2 was also observed in the previous DS plaque proteomics study (Supp. Table 18). Our study is consistent with previous similar proteomics studies on AD brains, and further expanded the proteins present at these pathological lesions.

Validation of CLCN6 and TPP1 in Aβ plaques by immunohistochemistry

We performed immunofluorescence to validate the late endosome protein CLCN6, as it emerged as the most abundant plaque protein among the top ten significantly altered proteins in DS Aβ plaques (Supp. Table 14). Previously, CLCN6 was identified within plaques solely through our

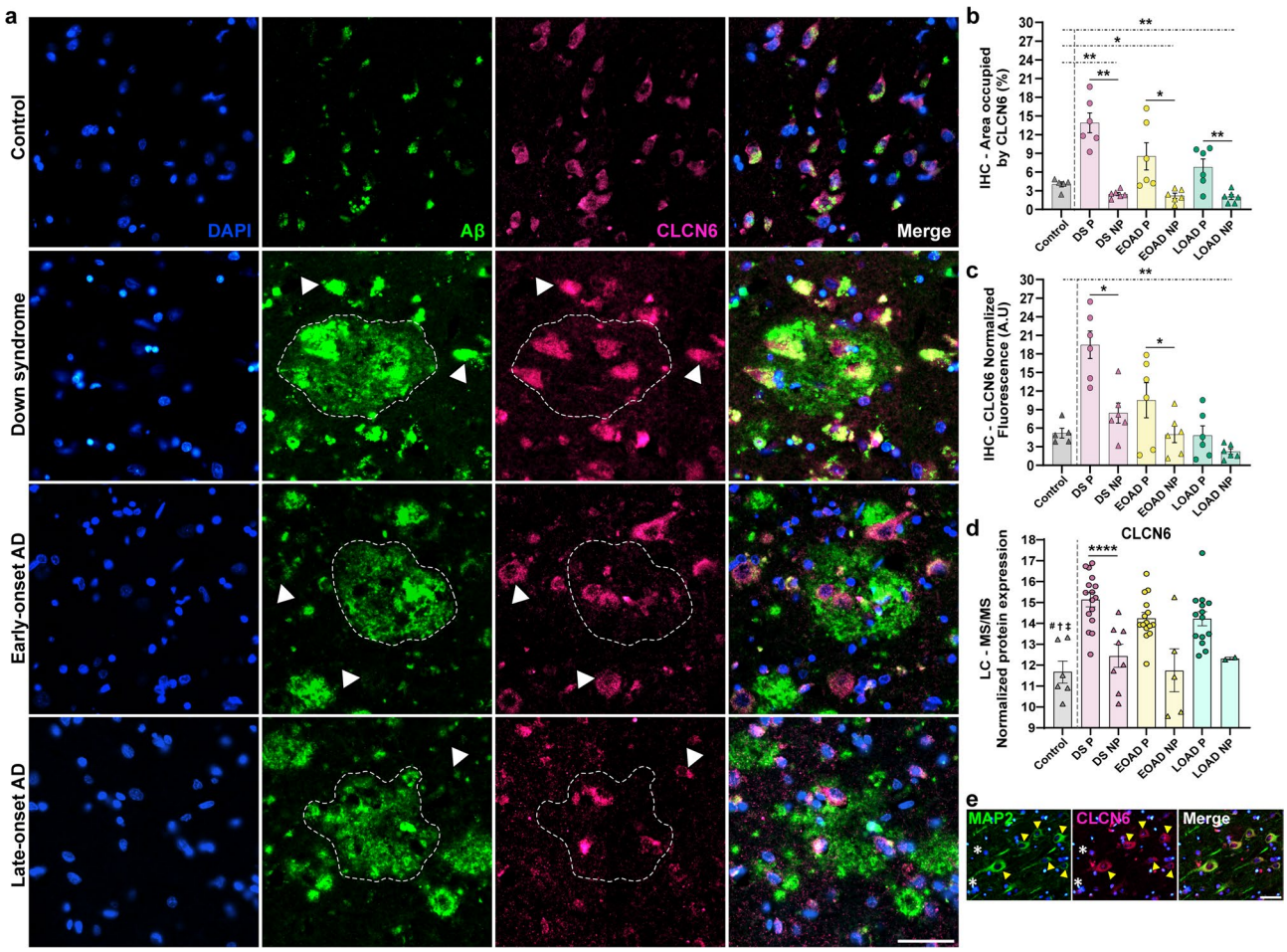

Fig. 9 Immunohistochemical validation of CLCN6 protein in human brain tissues. **a** Immunohistochemistry of Aβ and CLCN6 in control, DS, EOAD, and LOAD. Dotted line represents the plaque in CLCN6 panel. White arrowheads depict positive CLCN6 cells surrounding Aβ plaques. Merge panel shows intracellular colocalization of CLCN6 and Aβ. Scale bar 50 µm. **b** Bar graph showing normalized area occupied by CLCN6 and **c** normalized CLCN6 fluorescence, corresponding to plaque and non-plaque tissue. Paired two-tailed *t tests* indicate statistical differences between Plaque vs non-plaque tissue samples, whereas unpaired two-tailed *t tests* were performed to compare control non-plaque samples vs DS, EOAD, and LOAD non-plaque samples. For panels B and C, $n=6$ cases. **d** Normalized protein expression of CLCN6 obtained from the label-free quantitative mass spectrometry proteomics. **e** Immunohistochemistry of neuronal protein MAP2 and CLCN6 in DS tissue away from plaques. Yellow arrowheads depict co-staining of MAP2 and CLCN6. White asterisks show small unidentified cells negative for MAP2 and positive for CLCN6. Scale bar 50 µm. Pairwise comparisons p values are indicated. * $p<0.05$, ** $p<0.01$, **** $p<0.0001$. Error bars indicate standard error of the mean (SEM). Significant pairwise comparisons are indicated for those analyses that were performed, controls are shown as reference. Additional symbols on top of the control bar indicate that the given protein is not significantly abundant in non-plaque AD tissue compared to controls in # DS, † EOAD and ‡ LOAD, respectively

proteomics study [31], without histochemical evidence of its presence in Aβ plaques. Immunofluorescence staining showed CLCN6 localized in the cytoplasm of cells adjacent to intracellular 4G8 anti-Aβ-positive staining (Fig. 9a). Within plaques, Aβ appears to encapsulate CLCN6 + cells, with the highest intracellular colocalization between CLCN6 and Aβ. Moreover, CLCN6 + /4G8 + cells were observed on the periphery of amyloid plaques, suggesting a potential role for CLCN6 + cells in either releasing Aβ species into plaques or participating in a phagocytic process (Fig. 9a).

Quantification of CLCN6 fluorescence and area, normalized by plaque area, showed a significant increase in Aβ plaques in DS, EOAD, and LOAD compared to non-plaque tissue (Fig. 9b–c). Interestingly, CLCN6 area was significantly reduced in non-plaque tissue across all cohorts relative to control non-plaque tissue (Fig. 9b–c). These histochemical results are consistent with trends observed in the proteomic data (Fig. 9d). Further co-staining with MAP2 indicated that most CLCN6 + cells are neurons, with a minority of smaller MAP2- cells also displaying CLCN6 staining (Fig. 9e). Overall, these findings suggest that CLCN6 may be involved in storing and transporting Aβ, which could be released extracellularly in the AD pathogenic context, contributing to amyloid plaque formation.

TPP1 is a lysosomal protein that was identified in previous human proteomics [4, 31], but has not been characterized in Aβ plaques by immunohistochemistry. Our validation revealed a distinctive punctate expression pattern common of lysosomal-associated proteins. These bright puncta were consistently observed both within Aβ plaques and in the surrounding non-plaque regions (Fig. 10a). In addition to the punctate signal, TPP1 expression appeared to be widespread and highly abundant throughout the tissues, with immunoreactivity present diffusely in the cytoplasmic regions of presumably neurons and glial cells (Fig. 10a). We observed TPP1-positive staining in Aβ plaques, with a pattern suggesting that the protein is not directly colocalized with Aβ. Instead, TPP1 appears to occupy spaces within the plaques

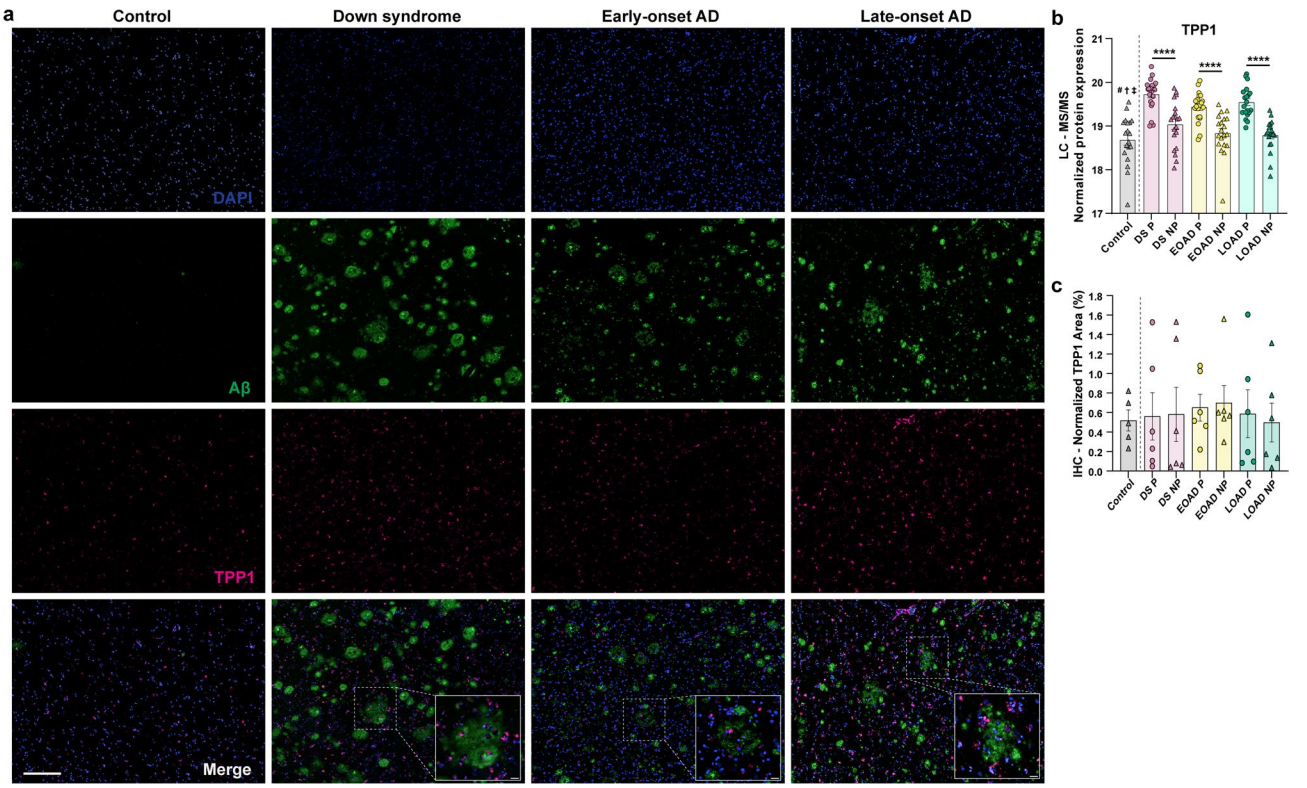

Fig. 10 Immunohistochemical validation of TPP1 protein in human brain tissues. **a** Immunohistochemistry of Aβ and TPP1 in control, DS, EOAD, and LOAD. Bottom panel, dotted lines highlight TPP1-positive immunolabeling embedded in Aβ plaques for DS, EOAD, and LOAD. Scale bar 200 µm and 20 µm for plaque zoom panels. **b** Normalized protein expression of TPP1 obtained from the label-free quantitative mass spectrometry proteomics. Pairwise comparisons *p* values are indicated. **** $p < 0.0001$. Significant pairwise comparisons are indicated for those analyses that were performed, controls are shown as reference. Additional symbols on top of the control bar indicate that the given protein is not significantly abundant in non-plaque AD tissue compared to controls in # DS, † EOAD, and ‡ LOAD, respectively. **c** Bar graph showing normalized TPP1 area, corresponding to plaque and non-plaque tissue. No statistical differences between plaque vs non-plaque tissue samples were found. For panels C, $n = 6$ cases. Error bars indicate standard error of the mean (SEM)

that are less densely packed with amyloid or is embedded within denser amyloid aggregates while remaining distinguishable (bottom panel Fig. 10a.). Our proteomics analysis showed that TPP1 is significantly enriched in plaques of DS, EOAD, and LOAD (Fig. 10b). However, the enrichment of TPP1 in amyloid plaques is low (fold-change of 1.62 in DS, 1.51 in EOAD, and 1.69 in LOAD; Supp. Table 3). We did not observe significant differences in TPP1 levels by IHC (Fig. 10c). Notably, the density and intensity of TPP1 staining within plaques were qualitatively similar to those in the non-plaque areas, consistent with proteomic findings indicating subtle enrichment of TPP1 in plaques. Overall, our observations suggest that TPP1 is not exclusively localized to plaques but is instead distributed throughout the brain parenchyma.

Correlation of protein changes to clinical traits

WGCNA allowed us to identify correlations between clusters of co-expressing proteins with clinical traits, including *APOE* genotype, sex, age, TDP-43 and α-synuclein copathologies, and Aβ and pTau pathology regional levels. Top GO BP and CC annotations associated with each module are presented (FDR < 0.05), with additional information about module sizes and extended functional annotation provided in the supplementary tables 19 to 26. Notably, Module 1 from DS plaques, containing multiple highly abundant plaque proteins (e.g., CLCN6, MDK, ITM2C, ARL8B, and C1QC), correlated significantly only with pTau levels ($R = 0.5$, $p = 0.024$) (Supp. Figure 4). In EOAD, we observed negative correlations between *APOE* 3 and 4 genotypes, as well as between *APOE* and age. Functional annotation indicated that modules correlated with *APOE* genotype are related to synaptic signaling and mitochondrial metabolic processes (Supp. Figure 5). Additionally, Module 5, including astrocytic proteins DES, VIM, GFAP, GJA1, and ALDH1L1, was positively correlated with *APOE3* and negatively correlated with *APOE4* ($R = 0.54$, $p = 0.014$ and $R = -0.52$, $p = 0.02$), underscoring astrocytes relevance in AD neuropathology (Supp. Figure 5). On the other hand, LOAD plaques co-expression networks revealed a significant correlation between Module 58, functionally associated with the axonal myelin sheath and containing multiple oligodendrocyte proteins (MOG, MBP, MAG, CNP, HAPLN2, and PLP1), and Aβ neuropathology ($R = -0.51$, $p = 0.021$) (Supp. Figure 6). In addition, Module 30, comprising proteins COL25A1, C3, and fibrinogens (FGA, FGB, FGG), was positively correlated with *APOE4* and Tau ($R = 0.45$, $p = 0.048$ and $R = 0.56$, $p = 0.01$, respectively), and negatively correlated with age ($R = -0.63$, $p = 0.011$) (Supp. Figure 6), suggesting potential age-dependent alterations in some of the proteins associated with module 30. Age correlated significantly with multiple modules in all cohorts, but it is noteworthy that the LOAD cohort is inherently older than DS and EOAD.

In non-plaque tissue co-expression networks, modules 15, 29, and 44 in DS non-plaques showed opposing correlations with *APOE3* and *APOE4* (Supp. Figure 7), with Module 15 also associated with "Cytoplasmic translation" and "Ribosomal subunit" functions. EOAD non-plaque networks showed the most modules significantly correlated with *APOE* genotype (Supp. Figure 8). Functional enrichment included terms related to neuron differentiation, axon structure, presynapse, cytoskeletal organization, and GTPase regulation in modules negatively correlated with *APOE4* (Supp. Figure 8). Module 55 was negatively correlated with *APOE4* and positively with Tau ($R = -0.57$, $p = 0.085$ and $R = 0.5$, $p = 0.025$) (Supp. Figure 8), and included proteins C3 and fibrinogens (FGA, FGB, FGG), similar to Module 30 in LOAD plaques. This observation suggests that common proteins may have distinct roles in AD pathology across subtypes. LOAD non-plaque correlation networks showed a few modules significantly correlated with *APOE4* genotype, similarly as LOAD plaques correlations (Supp. Figure 9). In particular, Module 23 was associated with "response to unfolded protein," comprising multiple heat shock proteins, such as HSPE1, HSPD1, HSPA8, HSPA9, and HSP90AA1 (Supp. Figure 9). Overall, our WGCNA analysis revealed that each cohort evaluated has distinct clusters of co-expressing proteins that correlate with clinical variables, such as *APOE* genotype, pTau, and Aβ pathology, suggesting that AD pathology progresses through different mechanisms in DS, EOAD, and LOAD. The interaction of the multiple proteins identified on each experimental group and clinical traits may inform the development of therapies and biomarkers tailored to each form of AD.

Discussion

We conducted a comparative analysis of Aβ plaque and non-plaque proteomes in individuals with DS, EOAD, and LOAD, identifying 43 proteins consistently altered in Aβ plaques across all cohorts. The Aβ plaque proteomes showed a high degree of correlation among DS and AD subtypes, although certain proteins showed differential abundance across the groups. GO functional enrichment and protein–protein interaction analyses indicated predominant associations of Aβ plaque proteins with APP metabolism, lysosomal functions, and immune responses. Our findings suggest a shared "Aβ plaque protein signature" across the evaluated groups, underscoring a notable similarity between the DS plaque proteome and those of EOAD and LOAD. In contrast, the non-plaque proteome showed group-specific variations in protein abundance, leading to distinct functional associations. These results highlight physiological

differences in the brains of individuals with DS compared to those with EOAD and LOAD.

Our unbiased localized proteomics approach enabled the identification of hundreds of proteins associated with Aβ plaques, including HTRA1, CLU, CLSTN1, GPC1, and VIM, which have been linked to protective roles against Aβ neuropathology or regulation of amyloid production [44, 73, 120, 125]. Additionally, we confirmed the presence of proteins in Aβ plaques that are less studied in the context of AD, such as CLCN6, ARL8B, TPP1, VAMP7, and SMOC1 [31], suggesting a potential important role for these proteins in AD pathology. We previously demonstrated a strong colocalization of SMOC1 with diffuse and neuritic plaques, with a higher proportion in hippocampus than in neighboring cortex [31]. Most recent findings have shown colocalization of SMOC1 and PDGFRα, indicating that SMOC1 expression is highest in OPCs, as expected from RNAseq datasets [5]. Furthermore, our findings include several previously unreported plaque-enriched proteins in human AD and DS proteomics, expanding on earlier studies. These novel proteins—linked to critical processes in AD pathology and DS, such as lysosomal function (ACP2, LAMTOR4), immune response (HLA-DRB5, IL36G), and ubiquitination (RBX1)—have been implicated in AD through genetic studies [20, 66, 87, 112, 123, 132, 135]. Thus, our results provide evidence supporting these proteins' involvement in AD pathophysiology.

Our network analysis revealed a functional pattern among plaque proteins, with an increased level of predicted protein–protein interactions observed across all experimental groups. Notably, proteins such as NTN1, NCSTN, SPON1, and CLSTN1 were present in all cohorts and have known associations with APP/Aβ processing [32, 47, 48, 77, 88, 94, 105, 111, 120, 134]. While APP metabolism is well recognized in AD, with the APP gene located on chromosome 21 [65], these APP-related proteins remain understudied in DS. Our proteomics data also highlighted the presence of immune and inflammation-related proteins, including C1QC, C4A, C3, MDK, CLU, HLA-DRB1, and HLA-DRB5. These proteins clustered near the APP node in the protein networks, suggesting potential interactions with Aβ. This observation aligns with prior studies linking complement proteins, CLU, and MDK to senile plaques [22, 74, 81]. Specifically, murine studies indicate that CLU may contribute to neurotoxicity and fibrillar Aβ deposition [26]. Conversely, MDK has been shown to bind Aβ, with transgenic mouse studies indicating a reduction in Aβ deposition, although the underlying mechanisms remain unclear [85]. Co-expression network analysis in murine AD models and human AD brain samples showed strong association of MDK with Aβ plaques and cerebrovascular amyloid (CAA), and suggest an increase in both parenchymal amyloid plaques and CAA, suggesting that MDK directly impacts amyloid deposition [74]. Furthermore, studies using AD mouse models suggest that complement proteins may contribute to synapse loss, dystrophic neurite formation, and increased Aβ aggregation, potentially through microglia–astrocyte crosstalk in response to amyloid pathology (reviewed by Batista and colleagues [7, 35, 56, 107, 131]). Additionally, our findings reveal the enrichment of HLA-DRB1 and the novel plaque-protein HLA-DRB5 in Aβ plaques. Previous single-cell transcriptomic studies of human AD prefrontal cortex have correlated HLA-DRB1 and HLA-DRB5 expression in microglia with AD pathology [80, 124], although the mechanisms of HLA proteins in Aβ neuropathology remain largely unknown.

Our Aβ plaques proteomics data highlighted the enrichment of multiple proteins associated with the endo/lysosomal pathway, supporting prior findings that lysosomal dysfunction is a fundamental mechanism in AD [17, 42, 86, 116]. We identified TPP1, PPT1, LAMP1, ARL8B, and confirmed VAMP7, previously identified as a novel amyloid plaque protein [31], which are involved in lysosomal trafficking, vesicle fusion and protein degradation [1, 100, 121]. ARL8B is associated with Niemann–Pick disease type C [99]. ARL8B also may have a neuroprotective role against amyloid pathology [46]. In addition, we showed that ARL8B is associated with plaques, specifically to areas that were not brightly stained for Aβ. In addition, we identified ARL8B expression in a subset of reactive plaque-associated astrocytes [31]. ARL8B has also been detected in cerebrospinal fluid of AD patients compared to controls and Huntington's disease patients, indicating that ARL8B altered levels are AD-specific [10]. LAMP1 has been found enriched in Aβ plaques, and studies using AD murine models have shown that LAMP1-plaque-associated protein is particularly increased in axons [43] and dystrophic neurites [108]. Additionally, there is an enrichment of LAMP1 in reactive microglia within senile plaques, which has been implicated in amyloid removal [6].

TPP1 is a lysosomal matrix protein and is ubiquitously expressed in the human brain [15]. TPP1 has been shown to destabilize Aβ through endoproteolytic cleavage [110], and deficiencies in TPP1, together with PPT1, are linked to the neurodegenerative lysosomal storage disease neuronal ceroid lipofuscinosis (NCL) [59]. TPP1 has been identified in previous human proteomics studies [4, 31], but our current work is the first to provide a preliminary characterization of its role in the context of AD plaque pathology. Label-free mass spectrometry is a highly sensitive technique, which explains our observation of a subtle but significant enrichment of TPP1 in plaques, despite that we did not have evidence of the same pattern in our histochemistry. Although our preliminary validation of TPP1 did not reveal significant differences between Aβ plaques and non-plaque tissue, we observed a punctate expression pattern throughout the brain parenchyma, with notable association to Aβ plaques. These findings are similar to

observations of other lysosomal proteins, such as ARL8B [31], LAMP1 [52], cathepsin D and lipofuscin [18], and CLCN6, which associate with plaques but do not directly colocalize with Aβ. This suggests that TPP1 may not interact directly with Aβ but is instead localized to small pockets within amyloid plaques where Aβ is either absent or undergoing degradation.

CLCN6 is predominantly expressed in neurons within the central and peripheral nervous systems and is localized in the late endosomes of neuronal cell bodies [92]. Our proteomics and immunohistochemical analyses confirmed the presence of CLCN6 in the neuronal cytoplasm, specifically surrounding intracellular Aβ, and revealed its enrichment in amyloid plaques compared to non-plaque tissue. Notably, CLCN6 has not been studied previously in the context of AD or DS, highlighting the novelty of these findings. Previous studies have demonstrated that CLCN6 disruption leads to lysosomal storage disease with behavioral abnormalities, resembling neuronal ceroid lipofuscinosis (NCL) [92, 95]. This pathology may be linked to a CLCN6 mutation impairing late endosome acidification, thereby compromising protein degradation and the autophagosomal pathway, which is a defect associated with late-onset NCL [103]. Late endosomes play a critical role in forming intraluminal vesicles and serve as reservoirs for sorting ubiquitinated proteins destined for lysosomal degradation. Disruption of CLCN6 may therefore impede the degradation of key proteins such as TDP-43 and Tau, potentially contributing to intracellular protein accumulation and drawing parallels with other neurodegenerative disorders [57, 103]. Additionally, our WGCNA analysis in DS plaques highlighted a co-expression network module, including CLCN6 and other highly abundant plaque proteins, associated with Tau neuropathology levels. Altogether, our data suggest that CLCN6 may play a substantial role in the aggregation of neurotoxic proteins associated with AD neuropathology through its function in the endo/lysosomal pathway.

A closer examination of the most significant functional associations in the DS Aβ plaque proteome elucidated a substantial enrichment of lysosomal-related GO terms, followed by those linked to the immune system and cell activation. Both lysosomal and immune processes are integral to AD pathophysiology [42, 69, 70, 81, 113, 116, 126]. Strong evidence suggests that endo/lysosomal alterations in DS are associated with APP and the βCTF fragment produced after BACE-1 cleavage of APP, potentially explaining early changes in DS [19, 58, 61, 62]. Increased systemic inflammation, possibly exacerbated by Aβ accumulation, is also evident in individuals with DS [34, 75]. Interestingly, the functional associations observed in the DS plaque proteome appear to be a combination of those found in EOAD and LOAD, further highlighting the Aβ plaque proteome similarity across cohorts.

Significant plaque proteins were enriched across all cohorts, with some proteins specifically enriched in certain groups. This may help understand AD pathogenesis and the unique mechanisms in DS and AD subtypes. Interestingly, COL25A1 (CLAC-P) was the most enriched protein in plaques, especially in DS compared to EOAD and LOAD. Previous studies in mice suggested that CLAC, derived from COL25A1, is crucial in converting diffuse Aβ deposits into senile plaques [51, 118]. This finding may partially account for the heightened amyloid pathology observed in DS. Moreover, previous research has shown that the interaction between CLAC and Aβ is determined by negatively charged residues in the central region [64]. Given recent discoveries about Aβ filaments in DS and Aβ fibril variation in different AD subtypes, structural differences in Aβ fibrils may result in unique interactions with COL25A1 [33, 97]. Further investigation is required to comprehend the binding affinity of COL25A1 in DS and other forms of AD. However, our previous study indicated similar levels of COL25A1 in DS and EOAD plaques [31]. It is plausible that the observed differences between our current and past studies are due to technical factors, such as sample preparation, data acquisition, and cohort size [98].

Our proteomics analysis revealed a significant reduction of oligodendrocyte proteins, including HAPLN2, PLP1, MOG, MAG, MBP, and BCAS1, within Aβ plaques and also in the non-plaque proteome across all cohorts compared to controls. Additionally, WGCNA analysis identified a co-expression module of these oligodendrocytic proteins that negatively correlates with Aβ neuropathology, suggesting that Aβ accumulation may impact oligodendrocyte function and myelin stability. Previous studies in the AD murine model 5xFAD reported loss of myelin-associated lipids and disruption of the myelin sheath associated with Aβ plaques in the brain parenchyma [67]. Zhan and colleagues provided evidence, using superior temporal gyrus of human AD brains, of increased levels of degraded MBP protein and colocalization with $A\beta_{42}$ in the plaque cores and also aggregated adjacent to the plaques [136]. Due to the interaction between MBP and $A\beta_{42}$, the authors suggest that degraded MBP and other damaged myelin components may have a role in plaque development [136]. These findings indicate that oligodendrocyte disruption may worsen neurodegeneration in the context of Aβ pathology and highlight a potential therapeutic target. A study in rhesus monkeys linked myelin degeneration to normal aging and cognitive decline [11]. Recent studies using transgenic mice and human AD tissues have shown that myelin defects promote Aβ plaque formation and cause transcriptional changes in oligodendrocytes seen in AD and other degenerative diseases [27, 101]. Given that individuals with DS often exhibit age-associated disorders earlier than euploid individuals [38], myelin damage may be an early characteristic in DS, potentially

exacerbating amyloid pathology. Further studies are warranted to understand how oligodendrocytes are impacted in DS and AD.

The analysis of the non-plaque tissue proteome in DS, EOAD, and LOAD highlighted two primary altered components in AD: the ECM and chromatin structure. In the DS non-plaque proteome, we observed a cluster of ECM-related proteins, which was not evident in EOAD and LOAD but suggested by functional annotation analysis. Early studies using human AD brain samples showed ECM proteins (collagen, laminin, and HSPG) colocalizing with neuritic plaques [90]. Subsequent findings in transgenic mice and human AD brain samples indicated increased mRNA levels of collagen-type VI proteins proportional to APP and Aβ expression, suggesting protective roles against Aβ neurotoxicity [21]. Our data indicate that the ECM in DS is more significantly affected compared to EOAD and LOAD. Recent studies using trisomy 21 iPSCs at different stages of neuronal induction suggested aberrant ECM pathways and increased cell–cell adhesion, affecting neural development [79, 83]. Proteomics studies of human AD brain tissues correlated cell–ECM interaction pathways and matrisome components with AD neuropathological and cognitive traits [63], and ECM components were observed in pre-clinical AD cases, suggesting early ECM alterations in AD. These observations support a more significant and earlier alteration of ECM proteins in DS, possibly exacerbated by AD neuropathology. Additionally, proteins linked to chromatin structure were consistently altered in non-plaque tissue in all groups, most prominently in LOAD and EOAD. Our observations align with previous research suggesting structural changes in chromatin accessibility and altered gene expression in AD [8, 78, 115, 122]. Studies using murine models of DS and trisomy 21 iPSCs have shown reduced global transcription activity and changes resembling those in senescent cells, such as chromosomal introversion, nuclear lamina disruption, and altered chromatin accessibility [82, 96]. This evidence may explain the differences observed in the protein interaction networks and functional annotation analyses between the non-plaque proteomes of DS and the AD subtypes studied.

While our study sheds light on the molecular mechanisms behind Aβ plaque pathology in DS and various forms of AD, it is essential to recognize certain limitations. Bottom–up proteomics identifies proteins from detected peptides, reflecting only the trypsin-digestible proteome. Proteins are assembled as the smallest set explaining all observed peptides, with specific proteoforms reported only if unique peptides are detected. Despite this limitation, bottom–up proteomics offers higher sensitivity than other methods and avoids the need for pre-selecting protein targets, making label-free mass spectrometry ideal for discovery proteomics. Our findings highlight significant proteome changes, providing a foundation for future hypothesis generation and further investigation into the mechanisms driving these protein alterations. However, future studies should use additional validation and characterization methods for candidate proteins, which could further substantiate our findings, such as evaluation by two-dimensional (2D) electrophoresis and Western blotting, in addition to immunohistochemistry. These top–down proteomic technologies will be helpful for quantifying the levels of specific proteins, thereby complementing the discovery-based approach of bottom–up proteomics and providing a more comprehensive view of protein isoforms and post-translational modifications.

Our analysis was also restricted to classic cored plaques and dense aggregates from DS and AD cases primarily at advanced disease stages, constraining our conclusions to an 'end-point' proteome profile. Nonetheless, we identified notable neuropathological distinctions between DS and other cohorts, potentially associated with observed proteomic alterations in plaque and non-plaque tissues. Future studies targeting different morphological types of plaques (i.e., diffuse or cotton-wool plaques) would be interesting. Our analysis was also limited to vulnerable brain regions in AD. Future investigations should encompass broader age ranges and include more detailed analysis of brain subregions, such as those within the hippocampus, entorhinal cortex, and adjacent temporal cortex. This approach could help create a more detailed 'proteomics landscape' of AD neuropathology, enhancing our understanding of disease progression and resilience mechanisms. Furthermore, membrane proteins, particularly integral membrane proteins, are often underrepresented in proteomics studies due to detection challenges. Finally, while our research is unbiased, it remains susceptible to variability arising from unknown genetic factors in each case. Subsequent research endeavors should integrate genetic details such as familial AD mutations and other known genetic variables, and expand on the sampling for *APOE* genotypes, to gain deeper insights into their impact on AD.

Conclusions

Our study provides novel insights into the amyloid plaque proteome of DS, highlighting key functional aspects and contrasting them with EOAD and LOAD. We observed a notable similarity among the plaque proteomes of DS, EOAD, and LOAD, with predominant associations of plaque proteins with endo/lysosomal pathways, immunity, and APP metabolism. Specifically, the identification of CLCN6 underscores its potential role in AD pathology through its involvement in the endo/lysosomal pathway and warrants further investigation as a potential therapeutic target. The analysis of the non-plaque proteome revealed significant differential

alterations in ECM and chromatin structure, emphasizing the nuanced differences between DS, EOAD, and LOAD. Our unbiased proteomics approach not only identifies enriched plaque proteins but also suggests potential therapeutic targets or biomarkers for AD, offering promising avenues for future research and clinical applications.

Supplementary Information The online version contains supplementary material available at https://doi.org/10.1007/s00401-025-02844-z.

Acknowledgements The authors wish to thank Jenny R Diaz for her valuable advice in writing the manuscript and Ludovic Debure for his technical assistance with this project. The authors also want to thank Dr. Eric Dammer for his valuable insights regarding weighted correlation network analysis for proteomics. Human post-mortem tissue was obtained from the NIH NeuroBioBank, the South West Dementia Brain Bank, University of Bristol, UK, member of the Brains for Dementia Research (BDR) Network, IDIBAPS Biobank from Barcelona, University of Pennsylvania, and NYU Grossman School of Medicine. The authors extend our gratitude to the families, clinicians, medical examiners, and coroners for their participation in this research.

Author contributions TW, MMA, and ED contributed to the conception and design of the research framework. MMA, EK, JS, AGP, and BU contributed to data collection. MMA, EK, and DL performed statistical analyses. MMA, DL, ED, JF, AL, and TW contributed to the interpretation of the data. MMA wrote the first draft of the manuscript. All authors contributed to the writing, critical review and editing of the manuscript. TW and EBL obtained funding.

Funding This manuscript was supported by NIH grants R01AG087280, P30AG066512 and P01AG060882 (to TW), and P30AG072979 (to EBL). The NYULH Center for Biospecimen Research and Development, Histology and Immunohistochemistry Laboratory (RRID:SCR_018304) is supported in part by the Laura and Isaac Perlmutter Cancer Center Support under Grant No. NIH/NCI P30CA016087. This study was also funded by the Instituto de Salud Carlos III (Ministerio de Asuntos Económicos y Transformación Digital, Gobierno de España) through the projects INT21/00073, PI20/01473 and PI23/01786 to J.F.) and the Centro de Investigación Biomédica en Red sobre Enfermedades Neurodegenerativas Program 1, partly jointly funded by Fondo Europeo de Desarrollo Regional, Unión Europea, Una Manera de Hacer Europa, and cofunded by the European Regional Development Fund/European Social Fund (ERDF/ESF), 'A way to make Europe'/'Investing in your future'. This work was also supported by the National Institutes of Health grants (R01 AG056850; R21 AG056974, R01 AG061566, R01 AG081394 and R61AG066543) to J.F. It was also supported by Fundación Tatiana Pérez de Guzmán el Bueno (IIBSP-DOW-2020-151 to J.F.) and Horizon 2020–Research and Innovation Framework Programme from the European Union (H2020-SC1-BHC-2018-2020 to J.F.).

Data availability The resulting mass spectrometry raw data are accessible on the MassIVE server (https://massive.ucsd.edu/) under MassIVE ID: MSV000094800. All data analyzed during this study are included in this published article and its supplementary information files.

Declarations

Conflict of interest J.F. reported receiving personal fees for service on the advisory boards, adjudication committees or speaker honoraria from AC Immune, Adamed, Alzheon, Biogen, Eisai, Esteve, Fujirebio, Ionis, Laboratorios Carnot, Life Molecular Imaging, Lilly, Lundbeck, Novo Nordisk, Perha, Roche, Zambón and outside the submitted work. J.F. reports holding a patent for markers of synaptopathy in neurodegenerative disease (licensed to ADx, EPI8382175.0).

References

1. Aladeokin AC, Akiyama T, Kimura A, Kimura Y, Takahashi-Jitsuki A, Nakamura H et al (2019) Network-guided analysis of hippocampal proteome identifies novel proteins that colocalize with Abeta in a mice model of early-stage Alzheimer's disease. Neurobiol Dis. https://doi.org/10.1016/j.nbd.2019.104603
2. Aldecoa I, Barroeta I, Carroll SL, Fortea J, Gilmore A, Ginsberg SD et al (2024) Down Syndrome biobank consortium: a perspective. Alzheimers Dement. https://doi.org/10.1002/alz.13692
3. Antonarakis SE, Skotko BG, Rafii MS, Strydom A, Pape SE, Bianchi DW et al (2020) Down syndrome. Nat Rev Dis Primers 6:9. https://doi.org/10.1038/s41572-019-0143-7
4. Askenazi M, Kavanagh T, Pires G, Ueberheide B, Wisniewski T, Drummond E (2023) Compilation of reported protein changes in the brain in Alzheimer's disease. Nat Commun 14:4466. https://doi.org/10.1038/s41467-023-40208-x
5. Balcomb K, Johnston C, Kavanagh T, Leitner D, Schneider J, Halliday G et al (2024) SMOC1 colocalizes with Alzheimer's disease neuropathology and delays Abeta aggregation. Acta Neuropathol 148:72. https://doi.org/10.1007/s00401-024-02819-6
6. Barrachina M, Maes T, Buesa C, Ferrer I (2006) Lysosome-associated membrane protein 1 (LAMP-1) in Alzheimer's disease. Neuropathol Appl Neurobiol 32:505–516. https://doi.org/10.1111/j.1365-2990.2006.00756.x
7. Batista AF, Khan KA, Papavergi MT, Lemere CA (2024) The importance of complement-mediated immune signaling in Alzheimer's disease pathogenesis. Int J Mol Sci. https://doi.org/10.3390/ijms25020817
8. Bendl J, Hauberg ME, Girdhar K, Im E, Vicari JM, Rahman S et al (2022) The three-dimensional landscape of cortical chromatin accessibility in Alzheimer's disease. Nat Neurosci 25:1366–1378. https://doi.org/10.1038/s41593-022-01166-7
9. Benjamini Y, Hochberg Y (2018) Controlling the false discovery rate: a practical and powerful approach to multiple testing. J Roy Stat Soc: Ser B (Methodol) 57:289–300. https://doi.org/10.1111/j.2517-6161.1995.tb02031.x
10. Boeddrich A, Haenig C, Neuendorf N, Blanc E, Ivanov A, Kirchner M et al (2023) A proteomics analysis of 5xFAD mouse brain regions reveals the lysosome-associated protein Arl8b as a candidate biomarker for Alzheimer's disease. Genome Med 15:50. https://doi.org/10.1186/s13073-023-01206-2
11. Bowley MP, Cabral H, Rosene DL, Peters A (2010) Age changes in myelinated nerve fibers of the cingulate bundle and corpus callosum in the rhesus monkey. J Comp Neurol 518:3046–3064. https://doi.org/10.1002/cne.22379
12. Braak H, Braak E (1991) Neuropathological stageing of Alzheimer-related changes. Acta Neuropathol 82:239–259. https://doi.org/10.1007/BF00308809
13. Brandt S, Jentsch TJ (1995) ClC-6 and ClC-7 are two novel broadly expressed members of the CLC chloride channel family. FEBS Lett 377:15–20. https://doi.org/10.1016/0014-5793(95)01298-2
14. Broly M, Polevoda BV, Awayda KM, Tong N, Lentini J, Besnard T et al (2022) THUMPD1 bi-allelic variants cause loss of tRNA acetylation and a syndromic neurodevelopmental disorder. Am J Hum Genet 109:587–600. https://doi.org/10.1016/j.ajhg.2022.02.001
15. Carcel-Trullols J, Kovacs AD, Pearce DA (2015) Cell biology of the NCL proteins: What they do and don't do. Biochim Biophys

Acta 1852:2242–2255. https://doi.org/10.1016/j.bbadis.2015.04.027
16. Castrillo JI, Lista S, Hampel H, Ritchie CW (2018) Systems biology methods for Alzheimer's disease research toward molecular signatures, subtypes, and stages and precision medicine: application in cohort studies and trials. Methods Mol Biol 1750:31–66. https://doi.org/10.1007/978-1-4939-7704-8_3
17. Cataldo AM, Barnett JL, Berman SA, Li J, Quarless S, Bursztajn S et al (1995) Gene expression and cellular content of cathepsin D in Alzheimer's disease brain: evidence for early up-regulation of the endosomal-lysosomal system. Neuron 14:671–680. https://doi.org/10.1016/0896-6273(95)90324-0
18. Cataldo AM, Hamilton DJ, Nixon RA (1994) Lysosomal abnormalities in degenerating neurons link neuronal compromise to senile plaque development in Alzheimer disease. Brain Res 640:68–80. https://doi.org/10.1016/0006-8993(94)91858-9
19. Cataldo AM, Peterhoff CM, Troncoso JC, Gomez-Isla T, Hyman BT, Nixon RA (2000) Endocytic pathway abnormalities precede amyloid beta deposition in sporadic Alzheimer's disease and Down syndrome: differential effects of APOE genotype and presenilin mutations. Am J Pathol 157:277–286. https://doi.org/10.1016/s0002-9440(10)64538-5
20. Chen Y, Neve RL, Liu H (2012) Neddylation dysfunction in Alzheimer's disease. J Cell Mol Med 16:2583–2591. https://doi.org/10.1111/j.1582-4934.2012.01604.x
21. Cheng JS, Dubal DB, Kim DH, Legleiter J, Cheng IH, Yu GQ et al (2009) Collagen VI protects neurons against Abeta toxicity. Nat Neurosci 12:119–121. https://doi.org/10.1038/nn.2240
22. Choi-Miura NH, Ihara Y, Fukuchi K, Takeda M, Nakano Y, Tobe T et al (1992) SP-40,40 is a constituent of Alzheimer's amyloid. Acta Neuropathol 83:260–264. https://doi.org/10.1007/BF00296787
23. Davidson YS, Robinson A, Prasher VP, Mann DMA (2018) The age of onset and evolution of Braak tangle stage and Thal amyloid pathology of Alzheimer's disease in individuals with Down syndrome. Acta Neuropathol Commun 6:56. https://doi.org/10.1186/s40478-018-0559-4
24. de Graaf G, Buckley F, Skotko BG (2017) Estimation of the number of people with Down syndrome in the United States. Genet Med 19:439–447. https://doi.org/10.1038/gim.2016.127
25. De Strooper B, Karran E (2016) The cellular phase of Alzheimer's Disease. Cell 164:603–615. https://doi.org/10.1016/j.cell.2015.12.056
26. DeMattos RB, O'Dell MA, Parsadanian M, Taylor JW, Harmony JA, Bales KR et al (2002) Clusterin promotes amyloid plaque formation and is critical for neuritic toxicity in a mouse model of Alzheimer's disease. Proc Natl Acad Sci U S A 99:10843–10848. https://doi.org/10.1073/pnas.162228299
27. Depp C, Sun T, Sasmita AO, Spieth L, Berghoff SA, Nazarenko T et al (2023) Myelin dysfunction drives amyloid-beta deposition in models of Alzheimer's disease. Nature 618:349–357. https://doi.org/10.1038/s41586-023-06120-6
28. Doellinger J, Schneider A, Hoeller M, Lasch P (2020) Sample preparation by easy extraction and digestion (SPEED): a universal, rapid, and detergent-free protocol for proteomics based on acid extraction. Mol Cell Proteomics 19:209–222. https://doi.org/10.1074/mcp.TIR119.001616
29. Dolfe L, Tambaro S, Tigro H, Del Campo M, Hoozemans JJM, Wiehager B et al (2018) The Bri2 and Bri3 BRICHOS domains interact differently with Abeta(42) and Alzheimer Amyloid Plaques. J Alzheimers Dis Rep 2:27–39. https://doi.org/10.3233/ADR-170051
30. Doran E, Keator D, Head E, Phelan MJ, Kim R, Totoiu M et al (2017) Down Syndrome, partial trisomy 21, and absence of Alzheimer's disease: the role of APP. J Alzheimers Dis 56:459–470. https://doi.org/10.3233/JAD-160836
31. Drummond E, Kavanagh T, Pires G, Marta-Ariza M, Kanshin E, Nayak S et al (2022) The amyloid plaque proteome in early onset Alzheimer's disease and Down syndrome. Acta Neuropathol Commun 10:53. https://doi.org/10.1186/s40478-022-01356-1
32. Edbauer D, Winkler E, Regula JT, Pesold B, Steiner H, Haass C (2003) Reconstitution of gamma-secretase activity. Nat Cell Biol 5:486–488. https://doi.org/10.1038/ncb960
33. Fernandez A, Hoq MR, Hallinan GI, Li D, Bharath SR, Vago FS et al (2024) Cryo-EM structures of amyloid-beta and tau filaments in Down syndrome. Nat Struct Mol Biol. https://doi.org/10.1038/s41594-024-01252-3
34. Flores-Aguilar L, Iulita MF, Kovecses O, Torres MD, Levi SM, Zhang Y et al (2020) Evolution of neuroinflammation across the lifespan of individuals with Down syndrome. Brain 143:3653–3671. https://doi.org/10.1093/brain/awaa326
35. Fonseca MI, Zhou J, Botto M, Tenner AJ (2004) Absence of C1q leads to less neuropathology in transgenic mouse models of Alzheimer's disease. J Neurosci 24:6457–6465. https://doi.org/10.1523/JNEUROSCI.0901-04.2004
36. Fortea J, Vilaplana E, Carmona-Iragui M, Benejam B, Videla L, Barroeta I et al (2020) Clinical and biomarker changes of Alzheimer's disease in adults with Down syndrome: a cross-sectional study. Lancet 395:1988–1997. https://doi.org/10.1016/S0140-6736(20)30689-9
37. Fortea J, Zaman SH, Hartley S, Rafii MS, Head E, Carmona-Iragui M (2021) Alzheimer's disease associated with Down syndrome: a genetic form of dementia. Lancet Neurol 20:930–942. https://doi.org/10.1016/S1474-4422(21)00245-3
38. Franceschi C, Garagnani P, Gensous N, Bacalini MG, Conte M, Salvioli S (2019) Accelerated bio-cognitive aging in Down syndrome: state of the art and possible deceleration strategies. Aging Cell. https://doi.org/10.1111/acel.12903
39. Gardiner K, Davisson M (2000) The sequence of human chromosome 21 and implications for research into Down syndrome. Genome Biol 1(reviews0002):0001. https://doi.org/10.1186/gb-2000-1-2-reviews0002
40. Glenner GG, Wong CW (1984) Alzheimer's disease and Down's syndrome: sharing of a unique cerebrovascular amyloid fibril protein. Biochem Biophys Res Commun 122:1131–1135. https://doi.org/10.1016/0006-291x(84)91209-9
41. Glenner GG, Wong CW (1984) Alzheimer's disease: initial report of the purification and characterization of a novel cerebrovascular amyloid protein. Biochem Biophys Res Commun 120:885–890. https://doi.org/10.1016/s0006-291x(84)80190-4
42. Gouras GK, Tsai J, Naslund J, Vincent B, Edgar M, Checler F et al (2000) Intraneuronal Abeta42 accumulation in human brain. Am J Pathol 156:15–20. https://doi.org/10.1016/s0002-9440(10)64700-1
43. Gowrishankar S, Yuan P, Wu Y, Schrag M, Paradise S, Grutzendler J et al (2015) Massive accumulation of luminal protease-deficient axonal lysosomes at Alzheimer's disease amyloid plaques. Proc Natl Acad Sci U S A 112:E3699-3708. https://doi.org/10.1073/pnas.1510329112
44. Grau S, Baldi A, Bussani R, Tian X, Stefanescu R, Przybylski M et al (2005) Implications of the serine protease HtrA1 in amyloid precursor protein processing. Proc Natl Acad Sci U S A 102:6021–6026. https://doi.org/10.1073/pnas.0501823102
45. Greenberg SG, Davies P, Schein JD, Binder LI (1992) Hydrofluoric acid-treated tau PHF proteins display the same biochemical properties as normal tau. J Biol Chem 267:564–569
46. Griffin EF, Yan X, Caldwell KA, Caldwell GA (2018) Distinct functional roles of Vps41-mediated neuroprotection in Alzheimer's and Parkinson's disease models of neurodegeneration. Hum Mol Genet 27:4176–4193. https://doi.org/10.1093/hmg/ddy308

47. Haass C, Schlossmacher MG, Hung AY, Vigo-Pelfrey C, Mellon A, Ostaszewski BL et al (1992) Amyloid beta-peptide is produced by cultured cells during normal metabolism. Nature 359:322–325. https://doi.org/10.1038/359322a0
48. Hafez DM, Huang JY, Richardson JC, Masliah E, Peterson DA, Marr RA (2012) F-spondin gene transfer improves memory performance and reduces amyloid-beta levels in mice. Neuroscience 223:465–472. https://doi.org/10.1016/j.neuroscience.2012.07.038
49. Handa T, Sasaki H, Takao M, Tano M, Uchida Y (2022) Proteomics-based investigation of cerebrovascular molecular mechanisms in cerebral amyloid angiopathy by the FFPE-LMD-PCT-SWATH method. Fluids Barriers CNS 19:56. https://doi.org/10.1186/s12987-022-00351-x
50. Hartley D, Blumenthal T, Carrillo M, DiPaolo G, Esralew L, Gardiner K et al (2015) Down syndrome and Alzheimer's Disease: common pathways, common goals. Alzheimers Dement 11:700–709
51. Hashimoto T, Fujii D, Naka Y, Kashiwagi-Hakozaki M, Matsuo Y, Matsuura Y et al (2020) Collagenous Alzheimer amyloid plaque component impacts on the compaction of amyloid-beta plaques. Acta Neuropathol Commun 8:212. https://doi.org/10.1186/s40478-020-01075-5
52. Hassiotis S, Manavis J, Blumbergs PC, Hattersley KJ, Carosi JM, Kamei M et al (2018) Lysosomal LAMP1 immunoreactivity exists in both diffuse and neuritic amyloid plaques in the human hippocampus. Eur J Neurosci 47:1043–1053. https://doi.org/10.1111/ejn.13913
53. Head E, Lott IT, Wilcock DM, Lemere CA (2016) Aging in Down syndrome and the development of Alzheimer's disease neuropathology. Curr Alzheimer Res 13:18–29. https://doi.org/10.2174/1567205012666151020114607
54. Heberle H, Meirelles GV, da Silva FR, Telles GP, Minghim R (2015) InteractiVenn: a web-based tool for the analysis of sets through Venn diagrams. BMC Bioinformatics 16:169. https://doi.org/10.1186/s12859-015-0611-3
55. Higginbotham L, Ping L, Dammer EB, Duong DM, Zhou M, Gearing M et al (2020) Integrated proteomics reveals brain-based cerebrospinal fluid biomarkers in asymptomatic and symptomatic Alzheimer's disease. Sci Adv. https://doi.org/10.1126/sciadv.aaz9360
56. Hong S, Beja-Glasser VF, Nfonoyim BM, Frouin A, Li S, Ramakrishnan S et al (2016) Complement and microglia mediate early synapse loss in Alzheimer mouse models. Science 352:712–716. https://doi.org/10.1126/science.aad8373
57. Hu YB, Dammer EB, Ren RJ, Wang G (2015) The endosomal-lysosomal system: from acidification and cargo sorting to neurodegeneration. Transl Neurodegener 4:18. https://doi.org/10.1186/s40035-015-0041-1
58. Im E, Jiang Y, Stavrides PH, Darji S, Erdjument-Bromage H, Neubert TA et al (2023) Lysosomal dysfunction in Down syndrome and Alzheimer mouse models is caused by v-ATPase inhibition by Tyr(682)-phosphorylated APP betaCTF. Sci Adv. https://doi.org/10.1126/sciadv.adg1925
59. Itagaki R, Endo M, Yanagisawa H, Hossain MA, Akiyama K, Yaginuma K et al (2018) Characteristics of PPT1 and TPP1 enzymes in neuronal ceroid lipofuscinosis (NCL) 1 and 2 by dried blood spots (DBS) and leukocytes and their application to newborn screening. Mol Genet Metab 124:64–70. https://doi.org/10.1016/j.ymgme.2018.03.007
60. Janoueix-Lerosey I, Pasheva E, de Tand MF, Tavitian A, de Gunzburg J (1998) Identification of a specific effector of the small GTP-binding protein Rap2. Eur J Biochem 252:290–298. https://doi.org/10.1046/j.1432-1327.1998.2520290.x
61. Jiang Y, Mullaney KA, Peterhoff CM, Che S, Schmidt SD, Boyer-Boiteau A et al (2010) Alzheimer's-related endosome dysfunction in Down syndrome is Abeta-independent but requires APP and is reversed by BACE-1 inhibition. Proc Natl Acad Sci U S A 107:1630–1635. https://doi.org/10.1073/pnas.0908953107
62. Jiang Y, Sato Y, Im E, Berg M, Bordi M, Darji S et al (2019) Lysosomal dysfunction in Down syndrome Is APP-dependent and mediated by APP-betaCTF (C99). J Neurosci 39:5255–5268. https://doi.org/10.1523/JNEUROSCI.0578-19.2019
63. Johnson ECB, Carter EK, Dammer EB, Duong DM, Gerasimov ES, Liu Y et al (2022) Large-scale deep multi-layer analysis of Alzheimer's disease brain reveals strong proteomic disease-related changes not observed at the RNA level. Nat Neurosci 25:213–225. https://doi.org/10.1038/s41593-021-00999-y
64. Kakuyama H, Soderberg L, Horigome K, Winblad B, Dahlqvist C, Naslund J et al (2005) CLAC binds to aggregated Abeta and Abeta fragments, and attenuates fibril elongation. Biochemistry 44:15602–15609. https://doi.org/10.1021/bi051263e
65. Kang J, Lemaire HG, Unterbeck A, Salbaum JM, Masters CL, Grzeschik KH et al (1987) The precursor of Alzheimer's disease amyloid A4 protein resembles a cell-surface receptor. Nature 325:733–736. https://doi.org/10.1038/325733a0
66. Karlsson IK, Ploner A, Wang Y, Gatz M, Pedersen NL, Hagg S (2023) Leukocyte DNA methylation in Alzheimer s disease associated genes: replication of findings from neuronal cells. Epigenetics 18:2158285. https://doi.org/10.1080/15592294.2022.2158285
67. Kaya I, Jennische E, Lange S, Tarik Baykal A, Malmberg P, Fletcher JS (2020) Brain region-specific amyloid plaque-associated myelin lipid loss, APOE deposition and disruption of the myelin sheath in familial Alzheimer's disease mice. J Neurochem 154:84–98. https://doi.org/10.1111/jnc.14999
68. Kent WJ, Sugnet CW, Furey TS, Roskin KM, Pringle TH, Zahler AM et al (2002) The human genome browser at UCSC. Genome Res 12:996–1006. https://doi.org/10.1101/gr.229102
69. Kinney JW, Bemiller SM, Murtishaw AS, Leisgang AM, Salazar AM, Lamb BT (2018) Inflammation as a central mechanism in Alzheimer's disease. Alzheimers Dement (N Y) 4:575–590. https://doi.org/10.1016/j.trci.2018.06.014
70. Krance SH, Wu CY, Chan ACY, Kwong S, Song BX, Xiong LY et al (2022) Endosomal-lysosomal and autophagy pathway in Alzheimer's Disease: a systematic review and meta-analysis. J Alzheimers Dis 88:1279–1292. https://doi.org/10.3233/JAD-220360
71. Leitner D, Kavanagh T, Kanshin E, Balcomb K, Pires G, Thierry M et al (2024) Differences in the cerebral amyloid angiopathy proteome in Alzheimer's disease and mild cognitive impairment. Acta Neuropathol 148:9. https://doi.org/10.1007/s00401-024-02767-1
72. Leitner D, Pires G, Kavanagh T, Kanshin E, Askenazi M, Ueberheide B et al (2024) Similar brain proteomic signatures in Alzheimer's disease and epilepsy. Acta Neuropathol 147:27. https://doi.org/10.1007/s00401-024-02683-4
73. Levin EC, Acharya NK, Sedeyn JC, Venkataraman V, D'Andrea MR, Wang HY et al (2009) Neuronal expression of vimentin in the Alzheimer's disease brain may be part of a generalized dendritic damage-response mechanism. Brain Res 1298:194–207. https://doi.org/10.1016/j.brainres.2009.08.072
74. Levites Y, Dammer EB, Ran Y, Tsering W, Duong D, Abreha M et al (2024) Integrative proteomics identifies a conserved Abeta amyloid responsome, novel plaque proteins, and pathology modifiers in Alzheimer's disease. Cell Rep Med. https://doi.org/10.1016/j.xcrm.2024.101669
75. Licastro F, Chiappelli M, Ruscica M, Carnelli V, Corsi MM (2005) Altered cytokine and acute phase response protein levels in the blood of children with Downs syndrome: relationship with dementia of Alzheimer's type. Int J Immunopathol

Pharmacol 18:165–172. https://doi.org/10.1177/039463200501800117
76. Lin PY, Chen LY, Jiang M, Trotter JH, Seigneur E, Sudhof TC (2023) Neurexin-2: an inhibitory neurexin that restricts excitatory synapse formation in the hippocampus. Sci Adv. https://doi.org/10.1126/sciadv.add8856
77. Lourenco FC, Galvan V, Fombonne J, Corset V, Llambi F, Muller U et al (2009) Netrin-1 interacts with amyloid precursor protein and regulates amyloid-beta production. Cell Death Differ 16:655–663. https://doi.org/10.1038/cdd.2008.191
78. Lukiw WJ, Crapper McLachlan DR (1990) Chromatin structure and gene expression in Alzheimer's disease. Brain Res Mol Brain Res 7:227–233. https://doi.org/10.1016/0169-328x(90)90032-9
79. Martinez JL, Piciw JG, Crockett M, Sorci IA, Makwana N, Sirois CL et al (2024) Transcriptional consequences of trisomy 21 on neural induction. Front Cell Neurosci 18:1341141. https://doi.org/10.3389/fncel.2024.1341141
80. Mathys H, Davila-Velderrain J, Peng Z, Gao F, Mohammadi S, Young JZ et al (2019) Single-cell transcriptomic analysis of Alzheimer's disease. Nature 570:332–337. https://doi.org/10.1038/s41586-019-1195-2
81. McGeer PL, Klegeris A, Walker DG, Yasuhara O, McGeer EG (1994) Pathological proteins in senile plaques. Tohoku J Exp Med 174:269–277. https://doi.org/10.1620/tjem.174.269
82. Meharena HS, Marco A, Dileep V, Lockshin ER, Akatsu GY, Mullahoo J et al (2022) Down-syndrome-induced senescence disrupts the nuclear architecture of neural progenitors. Cell Stem Cell 29(116–130):e117. https://doi.org/10.1016/j.stem.2021.12.002
83. Mollo N, Aurilia M, Scognamiglio R, Zerillo L, Cicatiello R, Bonfiglio F et al (2022) Overexpression of the Hsa21 Transcription Factor RUNX1 Modulates the Extracellular Matrix in Trisomy 21 Cells. Front Genet. https://doi.org/10.3389/fgene.2022.824922
84. Montine TJ, Phelps CH, Beach TG, Bigio EH, Cairns NJ, Dickson DW et al (2012) National Institute on Aging-Alzheimer's Association guidelines for the neuropathologic assessment of Alzheimer's disease: a practical approach. Acta Neuropathol 123:1–11. https://doi.org/10.1007/s00401-011-0910-3
85. Muramatsu H, Yokoi K, Chen L, Ichihara-Tanaka K, Kimura T, Muramatsu T (2011) Midkine as a factor to counteract the deposition of amyloid beta-peptide plaques: in vitro analysis and examination in knockout mice. Int Arch Med 4:1. https://doi.org/10.1186/1755-7682-4-1
86. Nixon RA (2017) Amyloid precursor protein and endosomal-lysosomal dysfunction in Alzheimer's disease: inseparable partners in a multifactorial disease. FASEB J 31:2729–2743. https://doi.org/10.1096/fj.201700359
87. Novikova G, Kapoor M, Tcw J, Abud EM, Efthymiou AG, Chen SX et al (2021) Integration of Alzheimer's disease genetics and myeloid genomics identifies disease risk regulatory elements and genes. Nat Commun 12:1610. https://doi.org/10.1038/s41467-021-21823-y
88. Park SY, Kang JY, Lee T, Nam D, Jeon CJ, Kim JB (2020) SPON1 can reduce amyloid beta and reverse cognitive impairment and memory dysfunction in Alzheimer's Disease mouse model. Cells. https://doi.org/10.3390/cells9051275
89. Paschen SA, Rothbauer U, Kaldi K, Bauer MF, Neupert W, Brunner M (2000) The role of the TIM8-13 complex in the import of Tim23 into mitochondria. EMBO J 19:6392–6400. https://doi.org/10.1093/emboj/19.23.6392
90. Perlmutter LS, Barron E, Saperia D, Chui HC (1991) Association between vascular basement membrane components and the lesions of Alzheimer's disease. J Neurosci Res 30:673–681. https://doi.org/10.1002/jnr.490300411
91. Perluigi M, Butterfield DA (2012) Oxidative stress and Down syndrome: a route toward Alzheimer-like dementia. Curr Gerontol Geriatr Res. https://doi.org/10.1155/2012/724904
92. Poet M, Kornak U, Schweizer M, Zdebik AA, Scheel O, Hoelter S et al (2006) Lysosomal storage disease upon disruption of the neuronal chloride transport protein ClC-6. Proc Natl Acad Sci U S A 103:13854–13859. https://doi.org/10.1073/pnas.0606137103
93. Potter H, Granic A, Caneus J (2016) Role of trisomy 21 mosaicism in sporadic and familial Alzheimer's disease. Curr Alzheimer Res 13:7–17. https://doi.org/10.2174/1567205013011512071006 16
94. Prasher VP, Farrer MJ, Kessling AM, Fisher EM, West RJ, Barber PC et al (1998) Molecular mapping of Alzheimer-type dementia in Down's syndrome. Ann Neurol 43:380–383. https://doi.org/10.1002/ana.410430316
95. Pressey SN, O'Donnell KJ, Stauber T, Fuhrmann JC, Tyynela J, Jentsch TJ et al (2010) Distinct neuropathologic phenotypes after disrupting the chloride transport proteins ClC-6 or ClC-7/Ostm1. J Neuropathol Exp Neurol 69:1228–1246. https://doi.org/10.1097/NEN.0b013e3181ffe742
96. Puente-Bedia A, Berciano MT, Tapia O, Martinez-Cue C, Lafarga M, Rueda N (2021) Nuclear Reorganization in Hippocampal Granule Cell Neurons from a Mouse Model of Down Syndrome: Changes in Chromatin Configuration. Int J Mol Sci, Nucleoli and Cajal Bodies. https://doi.org/10.3390/ijms22031259
97. Qiang W, Yau WM, Lu JX, Collinge J, Tycko R (2017) Structural variation in amyloid-beta fibrils from Alzheimer's disease clinical subtypes. Nature 541:217–221. https://doi.org/10.1038/nature20814
98. Rahman MM, Lendel C (2021) Extracellular protein components of amyloid plaques and their roles in Alzheimer's disease pathology. Mol Neurodegener 16:59. https://doi.org/10.1186/s13024-021-00465-0
99. Roney JC, Li S, Farfel-Becker T, Huang N, Sun T, Xie Y et al (2021) Lipid-mediated motor-adaptor sequestration impairs axonal lysosome delivery leading to autophagic stress and dystrophy in Niemann-Pick type C. Dev Cell 56(1452–1468):e1458. https://doi.org/10.1016/j.devcel.2021.03.032
100. Rosa-Ferreira C, Munro S (2011) Arl8 and SKIP act together to link lysosomes to kinesin-1. Dev Cell 21:1171–1178. https://doi.org/10.1016/j.devcel.2011.10.007
101. Sadick JS, O'Dea MR, Hasel P, Dykstra T, Faustin A, Liddelow SA (2022) Astrocytes and oligodendrocytes undergo subtype-specific transcriptional changes in Alzheimer's disease. Neuron 110(1788–1805):e1710. https://doi.org/10.1016/j.neuron.2022.03.008
102. Saini F, Dell'Acqua F, Strydom A (2022) Structural connectivity in Down Syndrome and Alzheimer's Disease. Front Neurosci. https://doi.org/10.3389/fnins.2022.908413
103. Sassi C, Capozzo R, Hammer M, Zecca C, Federoff M, Blauwendraat C et al (2021) Exploring dementia and neuronal ceroid lipofuscinosis genes in 100 FTD-like patients from 6 towns and rural villages on the Adriatic Sea cost of Apulia. Sci Rep 11:6353. https://doi.org/10.1038/s41598-021-85494-x
104. Serafini T, Kennedy TE, Galko MJ, Mirzayan C, Jessell TM, Tessier-Lavigne M (1994) The netrins define a family of axon outgrowth-promoting proteins homologous to C. elegans UNC-6. Cell 78:409–424. https://doi.org/10.1016/0092-8674(94)90420-0
105. Seubert P, Vigo-Pelfrey C, Esch F, Lee M, Dovey H, Davis D et al (1992) Isolation and quantification of soluble Alzheimer's beta-peptide from biological fluids. Nature 359:325–327. https://doi.org/10.1038/359325a0
106. Seyfried NT, Dammer EB, Swarup V, Nandakumar D, Duong DM, Yin L et al (2017) A Multi-network Approach Identifies Protein-Specific Co-expression in Asymptomatic and

Symptomatic Alzheimer's Disease. Cell Syst. https://doi.org/10.1016/j.cels.2016.11.006
107. Shah A, Kishore U, Shastri A (2021) Complement system in Alzheimer's disease. Int J Mol Sci. https://doi.org/10.3390/ijms222413647
108. Sharoar MG, Palko S, Ge Y, Saido TC, Yan R (2021) Accumulation of saposin in dystrophic neurites is linked to impaired lysosomal functions in Alzheimer's disease brains. Mol Neurodegener 16:45. https://doi.org/10.1186/s13024-021-00464-1
109. Snyder HM, Bain LJ, Brickman AM, Carrillo MC, Esbensen AJ, Espinosa JM et al (2020) Further understanding the connection between Alzheimer's disease and Down syndrome. Alzheimers Dement 16:1065–1077. https://doi.org/10.1002/alz.12112
110. Sole-Domenech S, Rojas AV, Maisuradze GG, Scheraga HA, Lobel P, Maxfield FR (2018) Lysosomal enzyme tripeptidyl peptidase 1 destabilizes fibrillar Abeta by multiple endoproteolytic cleavages within the beta-sheet domain. Proc Natl Acad Sci U S A 115:1493–1498. https://doi.org/10.1073/pnas.1719808115
111. Spilman PR, Corset V, Gorostiza O, Poksay KS, Galvan V, Zhang J et al (2016) Netrin-1 interrupts amyloid-beta amplification, increases sAbetaPPalpha in vitro and in vivo, and improves cognition in a mouse model of Alzheimer's Disease. J Alzheimers Dis 52:223–242. https://doi.org/10.3233/JAD-151046
112. Sun Y, Zhu J, Zhou D, Canchi S, Wu C, Cox NJ et al (2021) A transcriptome-wide association study of Alzheimer's disease using prediction models of relevant tissues identifies novel candidate susceptibility genes. Genome Med 13:141. https://doi.org/10.1186/s13073-021-00959-y
113. Szabo MP, Mishra S, Knupp A, Young JE (2022) The role of Alzheimer's disease risk genes in endolysosomal pathways. Neurobiol Dis. https://doi.org/10.1016/j.nbd.2021.105576
114. Szklarczyk D, Gable AL, Nastou KC, Lyon D, Kirsch R, Pyysalo S et al (2021) The STRING database in 2021: customizable protein-protein networks, and functional characterization of user-uploaded gene/measurement sets. Nucleic Acids Res 49:D605–D612. https://doi.org/10.1093/nar/gkaa1074
115. Tachiwana H, Dacher M, Maehara K, Harada A, Seto Y, Katayama R et al (2021) Chromatin structure-dependent histone incorporation revealed by a genome-wide deposition assay. Elife. https://doi.org/10.7554/eLife.66290
116. Takahashi RH, Milner TA, Li F, Nam EE, Edgar MA, Yamaguchi H et al (2002) Intraneuronal Alzheimer abeta42 accumulates in multivesicular bodies and is associated with synaptic pathology. Am J Pathol 161:1869–1879. https://doi.org/10.1016/s0002-9440(10)64463-x
117. Thal DR, Rub U, Orantes M, Braak H (2002) Phases of A beta-deposition in the human brain and its relevance for the development of AD. Neurology 58:1791–1800. https://doi.org/10.1212/wnl.58.12.1791
118. Tong Y, Xu Y, Scearce-Levie K, Ptacek LJ, Fu YH (2010) COL25A1 triggers and promotes Alzheimer's disease-like pathology in vivo. Neurogenetics 11:41–52. https://doi.org/10.1007/s10048-009-0201-5
119. Tyanova S, Temu T, Sinitcyn P, Carlson A, Hein MY, Geiger T et al (2016) The Perseus computational platform for comprehensive analysis of (prote)omics data. Nat Methods 13:731–740. https://doi.org/10.1038/nmeth.3901
120. Vagnoni A, Perkinton MS, Gray EH, Francis PT, Noble W, Miller CC (2012) Calsyntenin-1 mediates axonal transport of the amyloid precursor protein and regulates Abeta production. Hum Mol Genet 21:2845–2854. https://doi.org/10.1093/hmg/dds109
121. Vats S, Galli T (2022) Role of SNAREs in unconventional secretion-focus on the VAMP7-dependent secretion. Front Cell Dev Biol. https://doi.org/10.3389/fcell.2022.884020
122. Wang Y, Zhang X, Song Q, Hou Y, Liu J, Sun Y et al (2020) Characterization of the chromatin accessibility in an Alzheimer's disease (AD) mouse model. Alzheimers Res Ther 12:29. https://doi.org/10.1186/s13195-020-00598-2
123. Wang Z, Zhang Q, Lin JR, Jabalameli MR, Mitra J, Nguyen N et al (2021) Deep post-GWAS analysis identifies potential risk genes and risk variants for Alzheimer's disease, providing new insights into its disease mechanisms. Sci Rep 11:20511. https://doi.org/10.1038/s41598-021-99352-3
124. Wang ZX, Wan Q, Xing A (2020) HLA in Alzheimer's Disease: genetic association and possible pathogenic roles. Neuromolecular Med 22:464–473. https://doi.org/10.1007/s12017-020-08612-4
125. Watanabe N, Araki W, Chui DH, Makifuchi T, Ihara Y, Tabira T (2004) Glypican-1 as an Abeta binding HSPG in the human brain: its localization in DIG domains and possible roles in the pathogenesis of Alzheimer's disease. FASEB J 18:1013–1015. https://doi.org/10.1096/fj.03-1040fje
126. Webers A, Heneka MT, Gleeson PA (2020) The role of innate immune responses and neuroinflammation in amyloid accumulation and progression of Alzheimer's disease. Immunol Cell Biol 98:28–41. https://doi.org/10.1111/imcb.12301
127. Wegiel J, Kaczmarski W, Barua M, Kuchna I, Nowicki K, Wang KC et al (2011) Link between DYRK1A overexpression and several-fold enhancement of neurofibrillary degeneration with 3-repeat tau protein in Down syndrome. J Neuropathol Exp Neurol 70:36–50. https://doi.org/10.1097/NEN.0b013e318202bfa1
128. Wen Y, An Z, Qiao B, Zhang C, Zhang Z (2019) RPS7 promotes cell migration through targeting epithelial-mesenchymal transition in prostate cancer. Urol Oncol 37(297):e291-297. https://doi.org/10.1016/j.urolonc.2019.01.011
129. Wiseman FK, Pulford LJ, Barkus C, Liao F, Portelius E, Webb R et al (2018) Trisomy of human chromosome 21 enhances amyloid-beta deposition independently of an extra copy of APP. Brain 141:2457–2474. https://doi.org/10.1093/brain/awy159
130. Wisniewski T, Goni F (2015) Immunotherapeutic approaches for Alzheimer's disease. Neuron 85:1162–1176. https://doi.org/10.1016/j.neuron.2014.12.064
131. Wu T, Dejanovic B, Gandham VD, Gogineni A, Edmonds R, Schauer S et al (2019) Complement C3 is activated in human AD brain and is required for neurodegeneration in mouse models of amyloidosis and tauopathy. Cell Rep. https://doi.org/10.1016/j.celrep.2019.07.060
132. Xue J, Liu J, Geng M, Yue J, He H, Fan J (2021) Identification of potential hub genes of Alzheimer's disease by weighted gene co-expression network analysis. Nan Fang Yi Ke Da Xue Xue Bao 41:1752–1762. https://doi.org/10.12122/j.issn.1673-4254.2021.12.01
133. Yoshimura Y, Araki A, Maruta H, Takahashi Y, Yamashita H (2017) Molecular cloning of rat acss3 and characterization of mammalian propionyl-CoA synthetase in the liver mitochondrial matrix. J Biochem 161:279–289. https://doi.org/10.1093/jb/mvw067
134. Yu G, Nishimura M, Arawaka S, Levitan D, Zhang L, Tandon A et al (2000) Nicastrin modulates presenilin-mediated notch/glp-1 signal transduction and betaAPP processing. Nature 407:48–54. https://doi.org/10.1038/35024009
135. Yu L, Chibnik LB, Srivastava GP, Pochet N, Yang J, Xu J et al (2015) Association of Brain DNA methylation in SORL1, ABCA7, HLA-DRB5, SLC24A4, and BIN1 with pathological diagnosis of Alzheimer disease. JAMA Neurol 72:15–24. https://doi.org/10.1001/jamaneurol.2014.3049
136. Zhan X, Jickling GC, Ander BP, Stamova B, Liu D, Kao PF et al (2015) Myelin basic protein associates with AbetaPP, Abeta1-42, and amyloid plaques in cortex of Alzheimer's disease brain. J Alzheimers Dis 44:1213–1229. https://doi.org/10.3233/JAD-142013

137. Zhang B, Horvath S (2005) A general framework for weighted gene co-expression network analysis. Stat Appl Genet Mol Biol. https://doi.org/10.2202/1544-6115.1128
138. Zhang H, Meng L, Liu Y, Jiang J, He Z, Qin J et al (2023) Sfxn5 regulation of actin polymerization for neutrophil spreading depends on a citrate-cholesterol-PI(4,5)P2 pathway. J Immunol 211:462–473. https://doi.org/10.4049/jimmunol.2200863

Authors and Affiliations

Mitchell Martá-Ariza[1,2,3] · Dominique F. Leitner[1,2,4] · Evgeny Kanshin[5,6] · Jianina Suazo[1,2] · Ana Giusti Pedrosa[7] · Manon Thierry[1,2] · Edward B. Lee[8] · Orrin Devinsky[1,4] · Eleanor Drummond[2,9] · Juan Fortea[10,11,12] · Alberto Lleó[10,11] · Beatrix Ueberheide[1,5,6] · Thomas Wisniewski[1,2,13,14]

✉ Thomas Wisniewski
Thomas.wisniewski@nyulangone.org

1 Department of Neurology, NYU Grossman School of Medicine, New York, NY, USA

2 Center for Cognitive Neurology, NYU Grossman School of Medicine, New York, NY, USA

3 Institut de Neurociències, Universitat Autònoma de Barcelona, Barcelona, Spain

4 Comprehensive Epilepsy Center, Department of Neurology, NYU Langone Health and Grossman School of Medicine, New York, NY, USA

5 Proteomics Laboratory, Division of Advanced Research Technologies, NYU Grossman School of Medicine, New York, NY, USA

6 Department of Biochemistry and Molecular Pharmacology, NYU Grossman School of Medicine, New York, NY, USA

7 Center for Neural Science, New York University, New York, NY, USA

8 Department of Pathology and Laboratory Medicine, Perelman School of Medicine at the University of Pennsylvania, Philadelphia, PA, USA

9 Brain and Mind Centre and School of Medical Sciences, University of Sydney, Camperdown, NSW, Australia

10 Memory Unit, Department of Neurology, Institut de Recerca Sant Pau, Hospital de Sant Pau, Universitat Autònoma de Barcelona, Barcelona, Spain

11 Centro de Investigación Biomédica en Red en Enfermedades Neurodegenerativas (CIBERNED), Madrid, Spain

12 Barcelona Down Medical Center, Fundació Catalana de Síndrome de Down, Barcelona, Spain

13 Department of Pathology, NYU Grossman School of Medicine, New York, NY, USA

14 Department of Psychiatry, NYU Grossman School of Medicine, New York, NY, USA